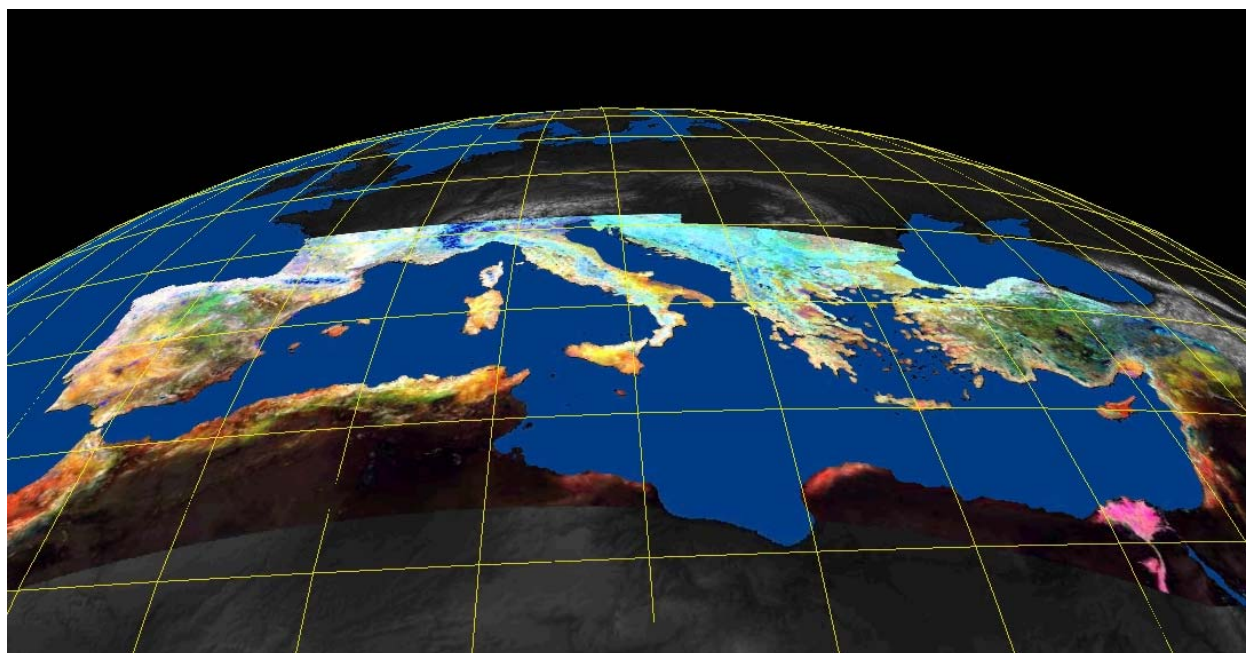# JRC Scientific and Technical Reports

Mediterranean-wide Green Vegetation Abundance for Land Degradation Assessment Derived from AVHRR NDVI and Surface Temperature 1989 to 2005

Weissteiner C. J., Böttcher K., Mehl W., Sommer S., Stellmes M.

JRC
EUROPEAN COMMISSION

ies
Institute for
Environment and
Sustainability

The mission of the Institute for Environment and Sustainability is to provide scientific-technical support to the European Union's Policies for the protection and sustainable development of the European and global environment.

***Europe Direct is a service to help you find answers
to your questions about the European Union***

Freephone number (*):

00 800 6 7 8 9 10 11

(*) Certain mobile telephone operators do not allow access to 00 800 numbers or these calls may be billed.

A great deal of additional information on the European Union is available on the Internet.
It can be accessed through the Europa server http://europa.eu/

Printed in Italy

Table of contents

Introduction

This work was mainly performed under the IP DESURVEY[1] project, a project contributing to the implementation of the actions 'Mechanisms of desertification' and 'Assessment of the vulnerability to desertification and early warning options' within the 'Global Change & Ecosystems priority'.

Within this project, as base data for a number of applications in the Mediterranean (e.g. erosion modelling, desertification syndrome modelling, hot spot detection, land use change, and trend analysis) an enhanced measure of vegetation density was needed. Using common vegetation indices like NDVI entail some limitations detecting thin vegetation cover, as it happens in areas of sparse vegetation found in arid areas or in areas vulnerable to desertification or land degradation.

The NDVI is known to be influenced by soil and rock background. Additionally, the NDVI shows sensitivity to several parameters such as the atmosphere, the illumination and the observation geometry, which is however supposed to be partly eliminated through a temporal maximum value compositing of the data (Holben, 1986). Moreover, the NDVI values are platform dependant due to different spectral properties as well as the observation geometry which complicates a direct comparison among different sensors. Due to these problems it is preferable to find a measure for vegetation abundance which is expected to be a better indicator for vegetation cover density.

In this context Linear Unmixing has been recognized as the most promising approaches for vegetation cover estimates, as shown in earlier studies (European Commission, 1998; Sommer, 1999). The applied unmixing technique is based on the inverse relationship between NDVI and land surface temperature. Generally, surface temperature (Ts) is observed to be inversely proportional to the amount of vegetation canopy cover and thus to the NDVI. This is due to a variety of factors including latent heat transfer through evapotranspiration, the lower heat capacity and thermal inertia of vegetation compared to soil (Choudhury, 1989; Goward & Hope, 1989).

The applied methodology to derive Green Vegetation Fraction (GVF) was expected to offer higher reliability and robustness than a simple vegetation index. It has been shown that using both NDVI and Ts, allows a characterization of land cover in a more comprehensive and climatically resistant manner than by multitemporal NDVI data alone (Nemani et al., 1993; Ehrlich & Lambin, 1996).

Since improved vegetation indices, like the JRC-FAPAR (Gobron et al., 2000) are not available for a long time span (FAPAR available from 1998 onwards) its use for long term assessments (e.g. trend analysis) are limited. Therefore a long term time series of AVHRR data with a time span of 17 years (1989 – 2005) was selected as base data set for the derivation of an enhanced vegetation abundance measure. The used base data set was the MEDOKADS data set (Koslowsky, 1998). Thanks to Freie Universität Berlin this dataset was recently updated and refined, putting strong effort to data pre-processing chain (Koslowsky, 2003). It consists of radiometrically and geometrically corrected data of all AVHRR channels, including derived data such as NDVI, surface temperature and meta data such as viewing angles or illumination geometry data. Despite its relatively coarse spatial resolution of 0.01 degrees (approx. 1 km^2) it does still offer one of the most valuable data sets for long term vegetation analysis.

---

[1] http://www.desurvey.net/

Algorithm overview

Objectives

The objective was to derive a measure of vegetation cover density for the Mediterranean, which can be derived for a long term remote sensing archive, such as NOAA/AVHRR. The parameter should lead to an improvement of the typical drawbacks of classical vegetation indices, especially in the context of scarcely vegetated areas. In view of a future extension, the methodology should also be applicable to sensors of newer generation, allowing the derivation of comparable results and potentially allow transferability.

Data characteristics

The AVHRR data set used covers the whole Mediterranean region [upper left corner 46° N, 10° W; lower right corner 27° N, 42° E (see Figure 4)]. This represents a subset of the original data, which is available also for regions further north.

The base data is provided by the MEDOKADS (Mediterranean Extended Daily One Km AVHRR Data Set) (Koslowsky et al., 2005). From this dataset 10-day-composites were used, computed according to Holben (1986) and matching the 1st, 11th and 21st of each month.

The data is provided as geographic lat/long WGS-1984 with a spatial resolution of 0.01 degrees.

The time series consists of AVHRR data of different NOAA satellites (NOAA11 for the time span 1989 - 1994, NOAA14 for the time span 1995 - 2000, NOAA16 for the time span 2001 to 2005).

The change from NOAA 14 (AVHRR/2) to NOAA 16 (AVHRR/3) was combined with a stronger spectral separation of the short wave channels 1 and 2 that led to an increase of the NDVI. The correction formulas published by Trishchenko et al. (2002) were applied to the data (channel 1 and 2) of NOAA 16 to account for it. In the case of the derived NDVI, the corrections seemed to be insufficient.

The calibration coefficients that were derived that account for the effects of sensor degradation to the shortwave channels of the AVHRR of the different NOAA satellites use an invariant target in the Western Great Erg desert in Algeria (Koslowsky et al., 2001). To remove the effects of changing illumination and observation geometry due to orbital shift, the effect of the BRDF (Bidirectional Reflectance Distribution Function) to the time series for the calibration target was removed by corrections for sun zenith angle (cosine correction) and normalization to nadir view conditions (Bolle et al., 2006). The slope of the regression lines for the time series of each satellite and for the whole time series of 17 years as well was forced to be zero. Thus artificial trends due to the characteristics of the different instruments are removed in the time series of the shortwave channels using the new calibration coefficients. As long as no BRDF corrections, mainly defined by surface and vegetation structure, are performed to the whole MEDOKADS area these effects are still included in the time series of selected targets.

The land surface temperature (Ts) is derived by the split window approach (Coll et al., 1994; Coll & Caselles, 1997) and normalized to the time of the local sun zenith plus 1 hour and 42 minutes (Billing, 2007).

Strategy

The status and dynamic of vegetation is usually assessed by vegetation indices (e. g. NDVI) when using NOAA-AVHRR data. Limitations for the detection of sparse vegetation with vegetation indices have been widely discussed in the literature. Several alternative indices, like GEMI (Pinty & Verstraete, 1992) or SAVI (Huete, 1988) have been developed to compensate for atmospheric and illumination conditions and soil background reflectance.

In this context spectral mixture analysis (SMA) has been applied by different authors [e. g. Smith et al. (1990); Hill et al. (1995)] to detect sparse vegetation cover from Landsat TM images in areas with spectrally diverse substrates. The difficulty encountered in the application of SMA to NOAA AVHRR data is related to the limited number of reflectance channels recorded and hence, restricts the separability of different surface materials.

Lambin and Ehrlich (1995) used the ratio between Ts and NDVI for continental scale land-cover classification and demonstrated a clear increase of biome discrimination when integrating both thermal information and vegetation index. Another technique to combine Ts and NDVI, is described hereafter. In contrast to the classical SMA approach, previous studies have used a modified unmixing approach with NOAA AVHRR data based on the inverse relationship between vegetation cover and the surface temperature under dry conditions (European Commission, 1998; Sommer, 1999).

Due to factors like the latent heat transfer through evapotranspiration, the lower heat capacity and the thermal inertia of vegetation compared to soil, the surface temperature is inversely proportional to the amount of vegetation canopy (Gates, 1980; Goward & Hope, 1989), which itself is proportional to the NDVI (Huete et al., 1987). On small spatial scale the variations of different vegetation species and soil classes can show a high variability regarding surface temperature (Choudhury, 1989), while on coarse geometric resolution (e.g. AVHRR) the variation seems to be primarily caused by the vegetation fraction, vegetation physiology and physiognomy being of secondary importance (Nemani et al., 1993). Thus, linear approximations to explain NDVI as well as surface temperature of mixed AVHRR pixel (vegetation and non-vegetation) in relation to vegetation have been given (Figure 1 and Figure 3). Fractional cover should predominantly control the position of an AVHRR land surface pixel in the feature space of NDVI and Ts. Water, surface moisture and local meteorological conditions may influence this position further.
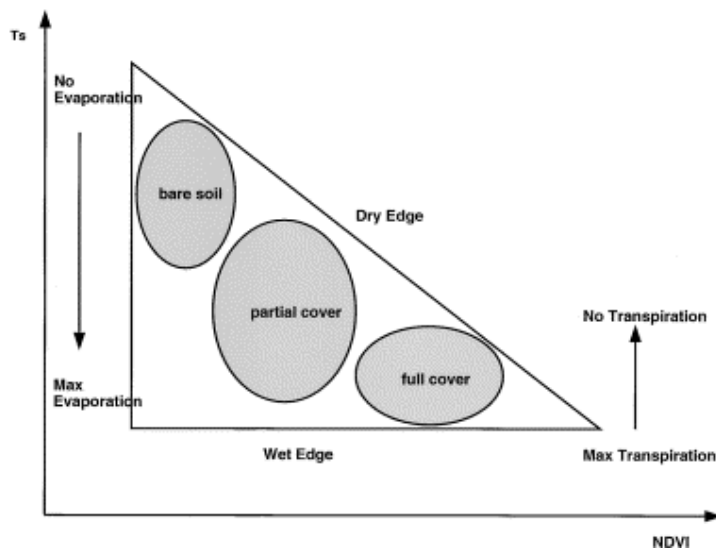

Figure 1 : Simplified Ts/NDVI (Lambin & Ehrlich, 1996; Sandholt et al., 2002)

Algorithm description

The concept of the classical linear spectral mixture analysis is based on the assumption, that the measured surface reflectance of a pixel is equivalent to the sum of the single reflectance from a limited number of pure materials - the so-called endmembers (EM) - depending on their pixel fraction (Adams & Smith, 1986). Mathematically, this assumption can be expressed as:

$$\rho_j = \sum_{i=1}^{m} F_i \cdot \rho e_{i,j} + \varepsilon_j \tag{1}$$

Where ρ_j denotes the reflectance of the mixed spectrum in band j, F_i the fraction of an endmember i of the pixel, $\rho e_{i,j}$ the reflectance of an endmember spectrum i in channel j and ε_j is the residual error in band j. At the same time the proportions of the endmember have to fulfill the sum-to-unity constraint, which can be expressed as:

$$\sum_{i=1}^{m} F_i = 1 \tag{2}$$

If the reflectance values of the endmembers are known, their fractions can be estimated for each pixel by solving a linear system of equations.
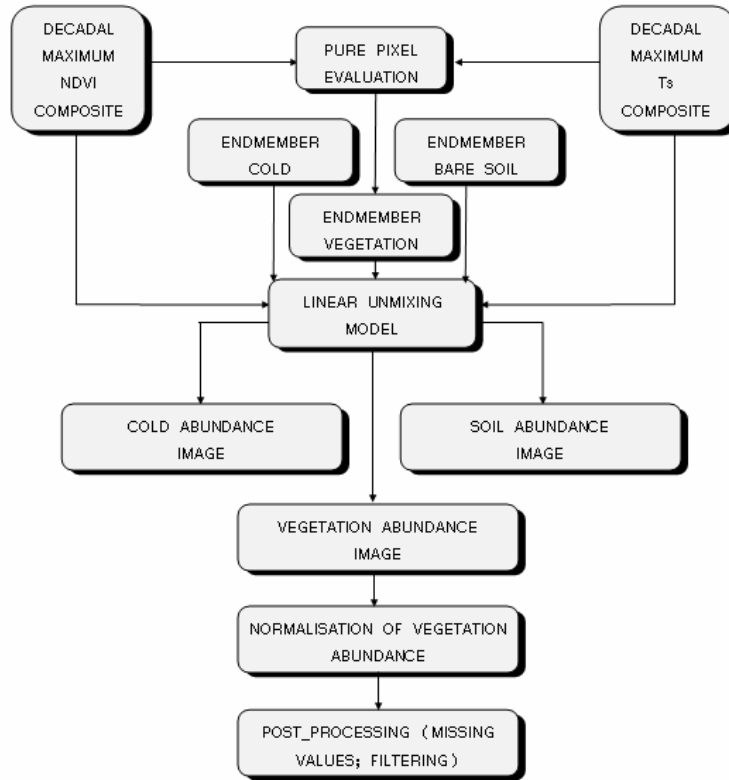

Figure 2 : Linear unmixing scheme applied to AVHRR time series for the assessment of vegetation coverage, after Sommer et al. (1999)

Instead of using reflectance characteristics like in the classical SMA approach (Adams & Smith, 1986), a spectral unmixing strategy was implemented based on the inverse relationship between the vegetation index NDVI and the land surface temperature as described before.

The scheme for the derivation of green vegetation fraction from the NOAA/AVHRR time series is given in Figure 2.

Technically, this approach derives three endmembers for each decade, the non-vegetated EM, the vegetated EM and the cold EM. These EMs represent the edges of the space spanned up by NDVI and surface temperature (Figure 1 and Figure 3) and therefore build a distinct and robust model to estimate the vegetation cover. The cold EM works similar to the shade EM in the common SMA, accounting for effects that lower the surface temperature of the surface, including local gradients related to altitude and exposition, temperature variations due to soil moisture, variable evaporation and transpiration respectively and remaining cloud artifacts.

Price (1993) expressed the NDVI of a mixed NOAA/AVHRR pixel as a function of the vegetation cover fraction as

$$NDVI_{pixel} = f \cdot NDVI_{veg} + (1-f) \cdot NDVI_{non-veg} \tag{3}$$

where $NDVI_{pixel}$ is the NDVI of a given pixel, f is the vegetation fraction, $NDVI_{veg}$ is the NDVI value for full vegetation and $NDVI_{non-veg}$ is the NDVI value for a non vegetated surface.
Likewise, the relationship between vegetation cover fraction and surface temperature was stated by Caselles and Sobrino (1989) as

$$T_{pixel} = f \cdot T_{veg} + (1-f) \cdot T_{non-veg} \tag{4}$$
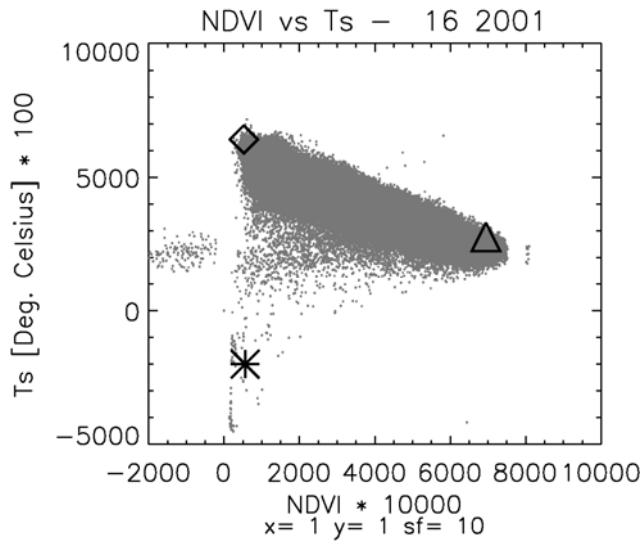
where T_{pixel} is the surface temperature of a pixel, f is the fraction of vegetation, T_{veg} the surface temperature for full vegetation and $T_{non-veg}$ denotes the surface temperature of a non vegetated surface. According to these relationships, the implemented spectral unmixing approach acts on the assumption that vegetation cover should predominantly control the position of an AVHRR land surface pixel within the feature space formed by NDVI and surface temperature (European Commission, 1998), which is illustrated by Figure 3.

Figure 3 : Unmixing triangle for a scatterplot consisting of the NDVI (x-axis) and Ts (y-axis) for the 16th decade 2001 (western Mediterranean window). EMs are depicted as symbols: non-vegetated EM (◇), vegetated EM (△) and cold EM (*).

Endmember selection from MEDOKADS data

For the determination of the three endmembers, the Mediterranean area was subdivided into an eastern and western window (Figure 4). This segmentation was introduced because the aforementioned vegetation – surface temperature relationship can strongly vary along the east-west gradient. Therefore, to improve the vegetation fraction estimation, this effect was accounted for by deriving the endmembers from a eastern and a western window. To avoid sharp transitions between the two tiles

for each pixel a linear interpolation of the derived endmembers was implemented. All criteria for the extraction of endmembers are documented in Table 1.
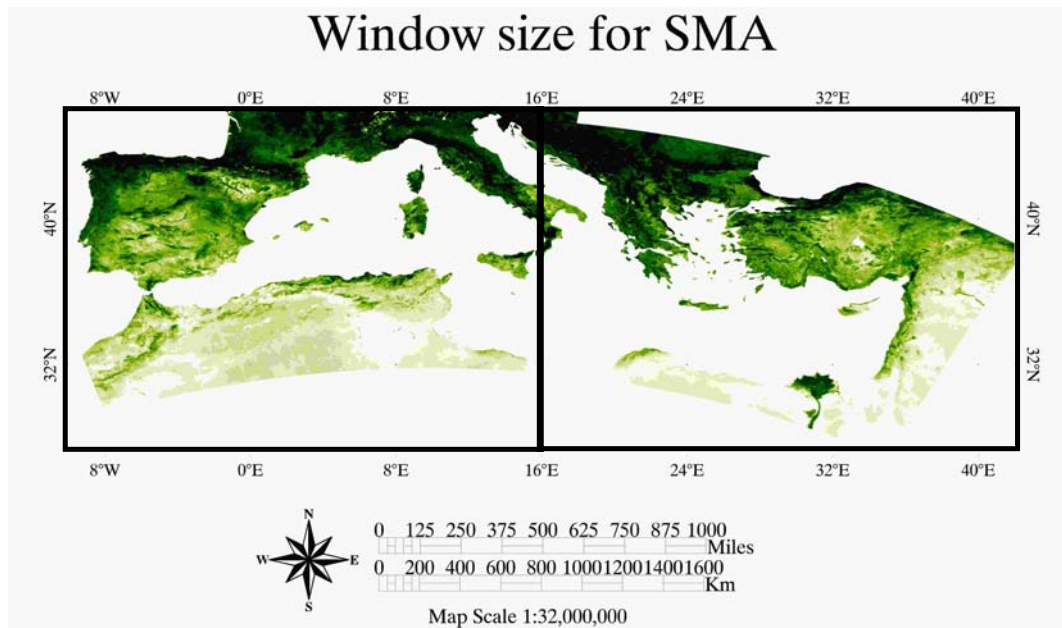

Figure 4 : Area covered for the study and subset windows used for the derivation of endmembers. The image depicts the derived average GVF for all years of the time series.

The NDVI-Ts relationship is not constant in time and space due to variable climatic conditions and the changing observation geometry. Therefore the "mixture triangle" has to be determined for each time step. An automated approach based on synthetic endmembers, following the method described by Stellmes et al. (2005), was applied. Endmembers were either defined upon theoretical considerations or extracted form the data using statistical methods.

In this context the NDVI value of the fully vegetated endmember was set to 0.7, which is the maximum NDVI value of vegetation for not atmospherically corrected NOAA AVHRR data according to literature (Czajkowski et al., 2004). To account for the dependency of the NDVI on the sun zenith angle (Θ_s)(Singh, 1988), the maximum possible NDVI value is corrected for each decade. The relationship between sun zenith angle and maximum NDVI has been determined empirically. To extract this relationship, the periods from 1989 – 2000 and 2001 – 2004 were analyzed.
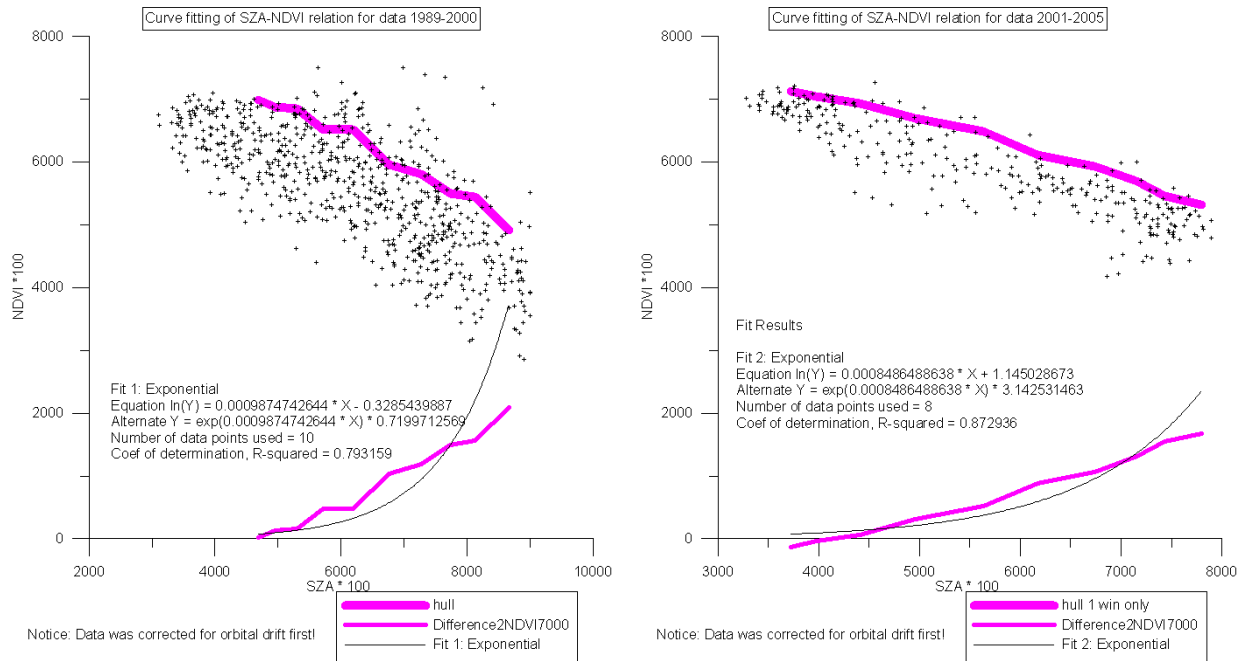
Figure 5 : Relationship of extracted maximum SZA and corresponding NDVI for each decade of (a) the time spans 1989 – 2000 and (b) 2001 – 2005. Also shown is the 'outer hull' of the NDVI/SZA values as well as the difference to the selected NDVI value of 0.7 and a fitted function at the lower part of the plots.

Although MEDOKADS data have been corrected for the SZA, a decline of NDVI with increasing SZA is clearly visible in Figure 5. As reported by Singh (1988), the reason for this might be atmosphere induced disturbances (ozone absorption, changing global irradiance and path radiance, water vapour) but also bidirectional effects (e.g. shadows) and the presence of non-Lambertian surfaces. As mentioned earlier, there was no atmospherical nor BRDF correction performed.

The separation into two periods should take into account the varying response of the AVHRR/2 and AVHRR/3 instruments in the red and near infrared band. Since the NDVI of bare soil is almost not affected by Θ_s, its NDVI was extracted at the lower edge of the decadal NDVI distribution (1 % percentile) of the whole Mediterranean dataset. To avoid the influence of remaining cloud pixels on the NDVI of the non-vegetated EM a temperature threshold was introduced (0° C). The NDVI of the cold EM was extracted separately for the eastern and western window at the lower edge of the decadal NDVI distribution (1 % percentile).

The temperatures of the fully vegetated and the non-vegetated EM were defined through the NDVI-Ts relationship. The relationship, which is described by a linear regression equation, was derived by the automatic approach described by Nemani (1993).

Modifying the initial method described by Stellmes et al.(2005), the temperature of the cold EM was set to a fixed value (-20 °C). Unlike other EMs, the cold EM can be considered as an artificial EM and is therefore less dynamic. The chosen temperature value represents occurring extreme values in the population of both windows (Eastern and Western Mediterranean).

Linear interpolation was applied for EM outliers in the temporal domain.

Table 1 : Selection criteria for endmembers in the NDVI-T$_S$ feature space

Endmember	NDVI	Ts
Non-vegetated	Based on percentile at the lower edge of NDVI values (1 %), considering positive NDVI values only. To avoid effects of remaining cloud pixels to the NDVI of the extracted non-vegetated EM, a threshold of 0 deg. C (lowest allowed value) was applied. One window for the whole area	Ts following Nemani (1993). Following this approach, the upperbound pixels of the Ts-NDVI scatter are extracted for each decade and fitted by a linear function. Gain and offset of this function are used to derive the temperature of the given NDVI. Number of window(s): n=2
Fully vegetated	Max. NDVI is set to 0.7 and corrected then for the relationship sun zenith angle (corrected for orbital drift) versus NDVI (Holben and Fraser 1984, Singh 1988) - empirical approach, defined separately for the two time periods 1989-2000 and 2001-2004 Number of window(s): n=2,	Ts following Nemani (1993). Following this approach, the upperbound pixels of the Ts-NDVI scatter are extracted for each decade and fitted by a linear function. Gain and offset of this function are used to derive the temperature of the given NDVI. Number of window(s): n=2,
Cold	Based on percentile at the lower edge of NDVI values (1 %) Number of window(s): n=2,	-20 degrees C Number of window(s): n=2

Figure 6 and Figure 7 depict EMs for decades of the year 2001 for the Eastern and Western Mediterranean. The coordinates of the EMs in the NDVI-Ts feature space are shown in Figure 6. The temporal run of the EMs is given in Figure 7. The NDVI for the fully vegetated EM follows a smooth run throughout the year, depending on the sun zenith angle. Ts values for the non-vegetated EMs are reaching a distinct peak in summer, whereas the Ts value of the fully vegetated EM shows smaller variation throughout the year. The cold EM run gives variations for NDVI only (temperature was fixed).
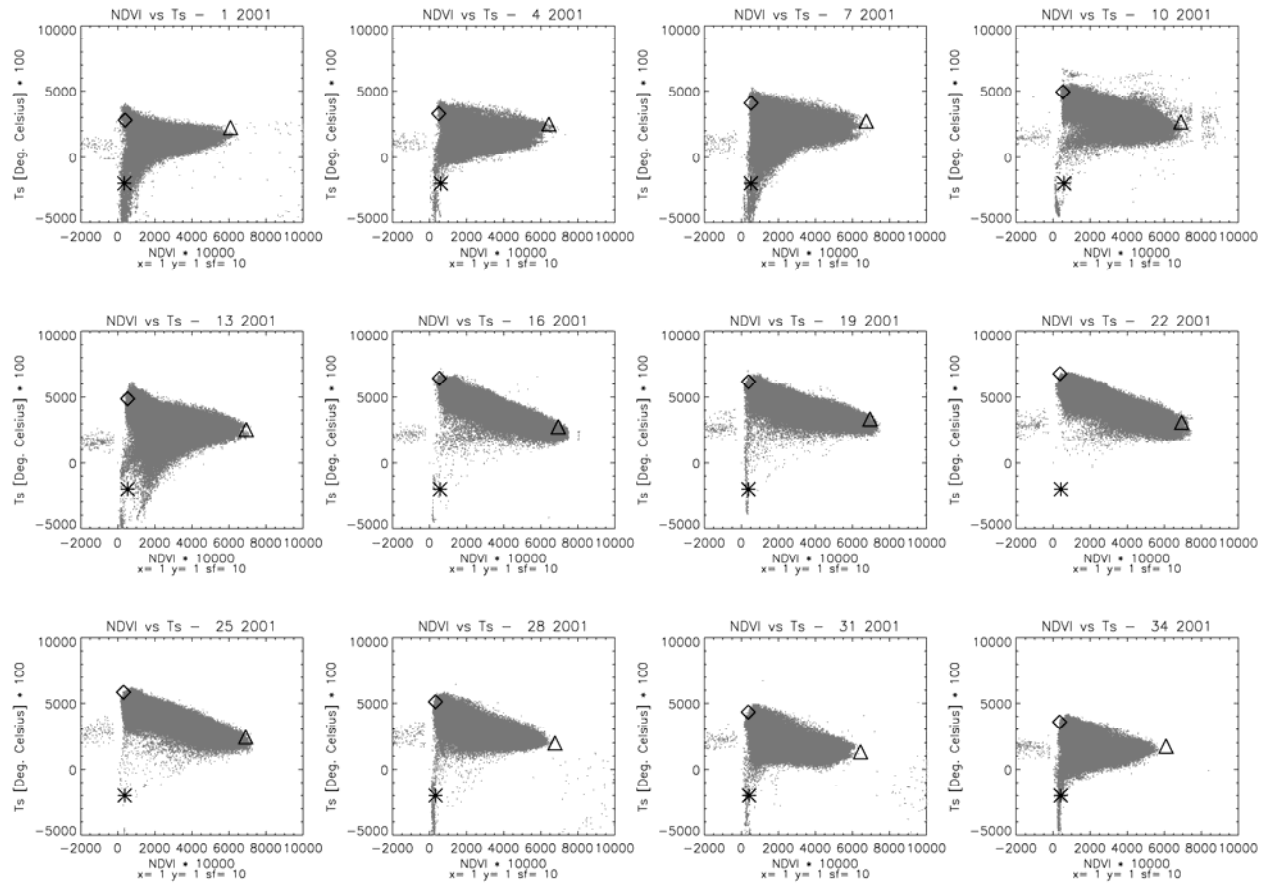
Figure 6 : Scatterplots for the NDVI (x-axis) – Ts (y-axis) relationship for 12 decades (first decade of a month at a time) of the year 2001 (western window). The number of decade is indicated in each title. EMs are depicted as symbols: non-vegetated EM (◊), vegetated EM (Δ) and cold EM (*).
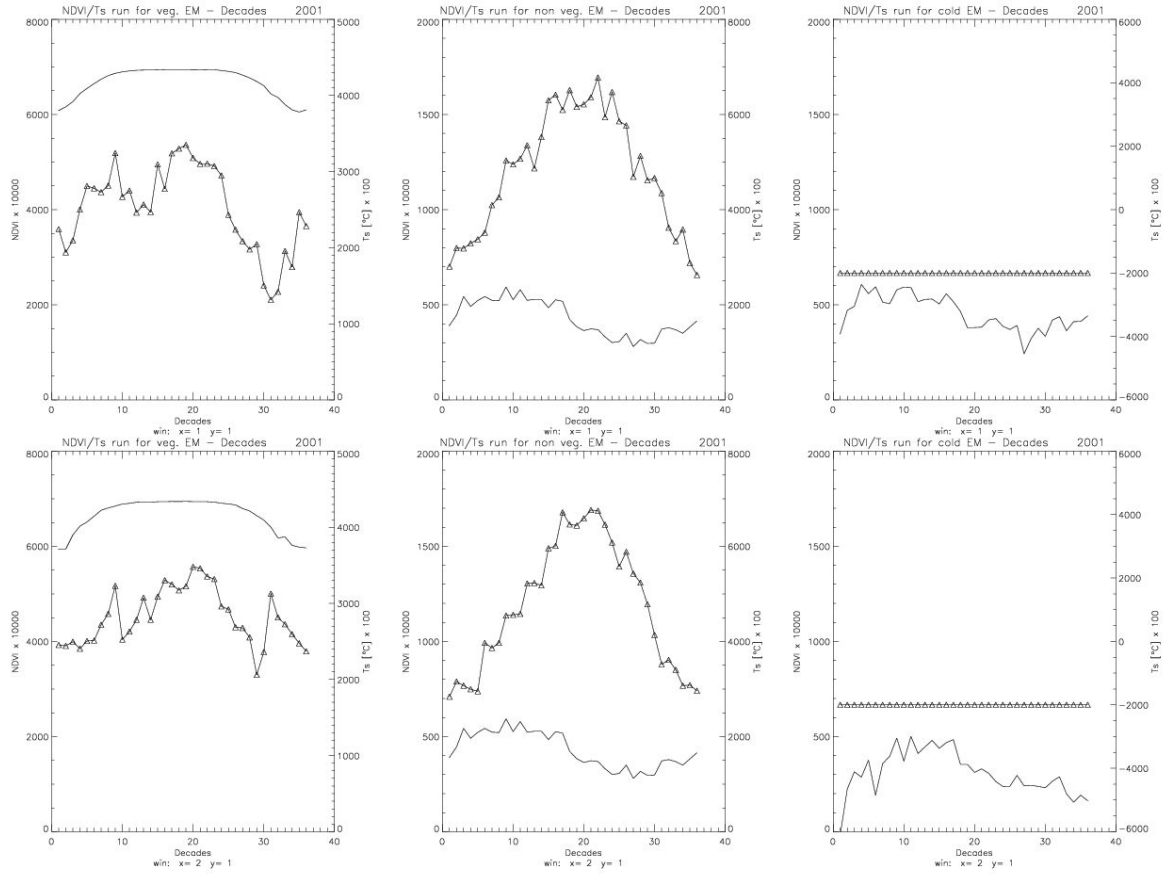
Figure 7 : Multi-temporal NDVI-(-) and Ts-run (Δ) for vegetated EM (1ˢᵗ column), non-vegetated EM (2ⁿᵈ column) and cold EM (3ʳᵈ column) for the year 2001. The first row depicts EMs for the Western, the 2ⁿᵈ row for the Eastern Mediterranean.

Unmixing

Prior to linear unmixing, the initially discrete number of chosen EMs (i.e. 3 EMs times 2 windows) were interpolated spatially (linearly) for each pixel, setting the EMs as central window pixels.

The computation of proportional abundance can be principally explained and solved with a simple system of linear equations as follows:

$$A \cdot X = B \tag{5}$$

where A = m (channels) * n (endmember) matrix of spectral endmembers
   X = n * 1 unknown vector of abundances
   B = m * 1 observed data vector (mixed pixel NDVI and Ts)

The unknown vector of abundances is determined by inverting the endmember matrix A:

$$X = A^{-1} \cdot B \tag{6}$$

A unique solution is possible if the number of spectral endmembers corresponds to the number of spectral bands. Furthermore in the case of an underdetermined problem (this study) the number of unknown endmembers exceeds the number of bands by one, a solution can be found by assuming the set of endmembers is exhaustive (i. e., the sum of the computed endmember fractions is equal to one).

The unmixing procedure resulted in the three abundances images for each decade: the vegetation, non-vegetated (soil) and "cold" abundance.

Normalization of the vegetation abundance

The vegetation abundance was normalized according to the assumption that the "cold" component does not change the ratio between the other derived abundances. The abundance of the cold endmember was apportioned to the remaining endmembers by taking into account their fractional abundance through the following factor:
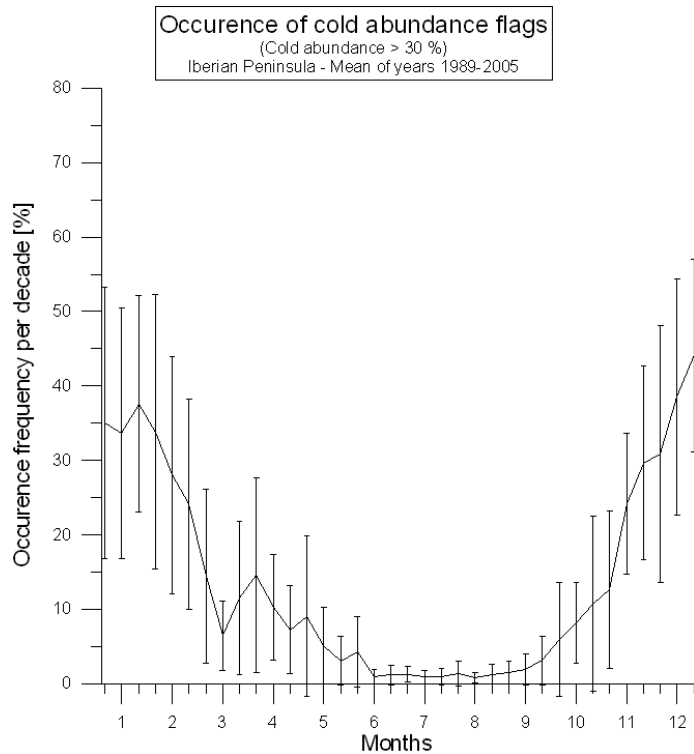
$$F = 1/(1 - F_{cold})$$ (7)

This is applied up to a cold abundance of 30 %. If the cold abundance exceeds this value, this GVF modeling approach is rejected as invalid and these pixels are flagged as NODATA. The value 30 % was chosen, as it represents a value, when the cold EM starts getting predominant and this implies that the assumption of an inverse NDVI-Ts-relationship starts getting questionable. It was found for the Iberian Peninsula that the number of pixels above this threshold did not exceed 15 % during the period March – October, averaged over all years 1989 – 2005 (see Figure 8).

The terms normalized vegetation abundance and green vegetation fraction (GVF) will be used equally in this document.

Figure 8 : Occurrence of cold abundance greater than 30 %.

Post-Processing of the GVF time series

Most post processing steps were carried out with the non-commercial software TIMESTATS developed by Thomas Udelhoven (Udelhoven, 2006).

Missing data were substituted by the seasonal mean of the time series.

Outliers were identified according to the *Chebyshev's Theorem,* which states that a random variable will take on a value within k standard deviations s of the mean with a probability of at least $(1- 1/k^2)$ (Lohninger, 1999). The probability (confidence interval) has been set to 0.95, which corresponds to a k of 4.5. Outliers were replaced, by the seasonal mean of pixel.

Filtering was applied using a the *Savitzky-Golay*-filter (Chen et al., 2004). The window size was set to 6 decades in forward and backward direction. Polynomial degree was chosen as 2.

Practical consideration

As described above, data gaps and outliers were filled with seasonal means of the remaining years. Additionally, data filtering occurred. In most cases data gaps consisted of a single decadal gap. In few cases, however, longer gaps had to be filled. This was the case between the 17th decade 1990 and the 6th decade 1991, between the 26th decade 1994 and the 4th decade 1995 and between the 25th decade and the 36th decade 2005 (see Figure 9).
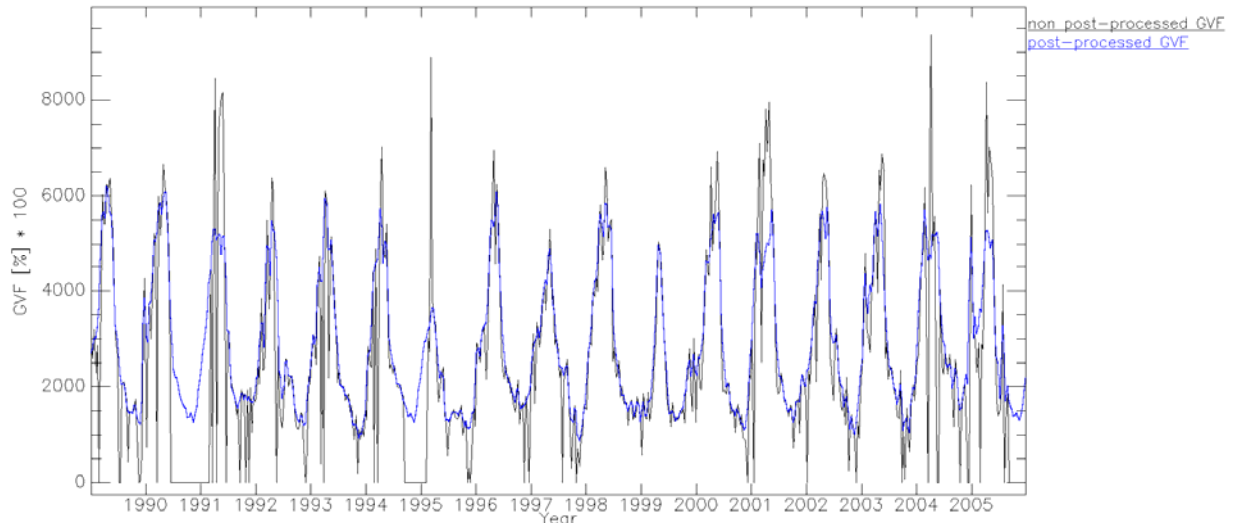

Figure 9 : Typical time series profile of non post-processed GVF data (blue line) in comparison with post-processed data (black line). A value of 0 of the non post-processed time series indicates missing values for this pixel.

The output data is in ENVI format (binary files with ENVI header files). The data is coded as integer values, GVF being expressed as % times 100. A value of 20 % GVF has the value 2000. NoData values are coded as 0. All data has remained un-projected in lat-long WGS-1984, spatial resolution is 0.01 degrees, as the original data is.

The output generated by the unmixing algorithm consists in four stacked abundance images: the normalised (GVF) and non-normalised green vegetation abundance, the soil (background) abundance and the "cold" abundance, each data set consisting of 612 layers (17 years * 36 decades per year).
The data is available for scientific purposes. Free download of the data is foreseen from the website http://desert.jrc.ec.europa.eu. For further information contact the authors of this report.

Results

As an example for the derived data set, a colour combination of three decadal values of GVF from year 1989, covering the whole Mediterranean, is shown in Figure 10. The colored map, which is composed of three decades, depicts only a small part of the information, which this contained especially in the time domain of the time series.
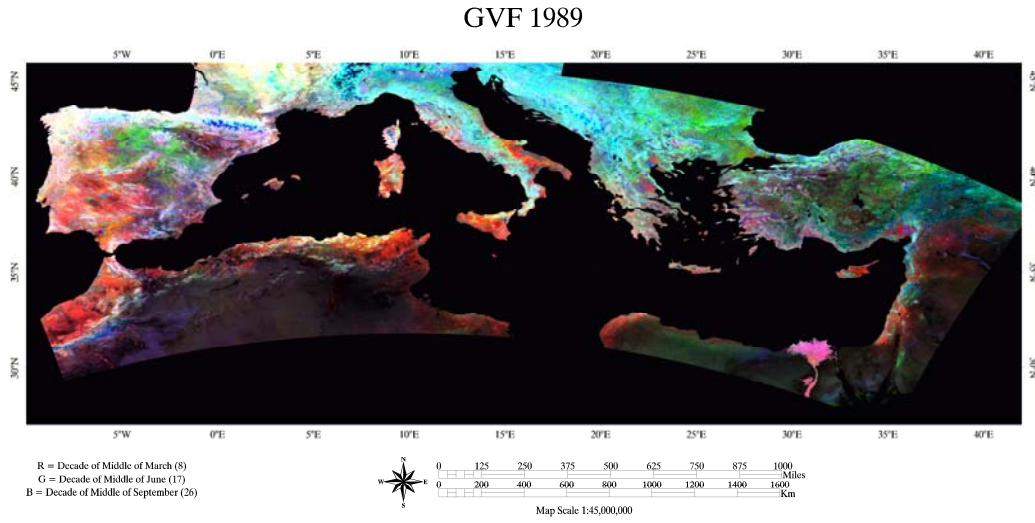
GVF 1989

R = Decade of Middle of March (8)
G = Decade of Middle of June (17)
B = Decade of Middle of September (26)

Map Scale 1:45,000,000

Figure 10 : RGB-composite of green vegetation abundance for three decades of the year 1989. Decade 8 (2nd decade March) is colored red, decade 17 (2nd decade June) green and decade 26 (2nd decade September) colored blue. Color saturation of the respective decade indicate highest values.

GVF was tested over different test sites. An overall comparison was carried out for the Iberian Peninsula, disregarding specific land cover. For more detailed analysis, test sites of specific properties have been chosen. The aim was to test and compare GVF on sites with different amounts of vegetation cover and vegetation dynamics within the growing cycle. Additionally, GVF was compared with independently derived high and low resolution vegetation cover (fCover).

NDVI-GVF Relationship

For the comparison of GVF with NOAA/AVHRR NDVI, the original NDVI and a scaled NDVI has been included in the analysis.

Scaled NDVI values for each pixel were computed as follows:

$$NDVI_{scaled,i} = \frac{NDVI_i - NDVI\,EM_{non-veg}}{NDVI\,EM_{veg} - NDVI\,EM_{non-veg}} \qquad\qquad 0 \leq NDVI_{scaled,i} \leq 1 \qquad (8)$$

where $NDVI_{scaled}$ = scaled NDVI
$NDVI$ = original NDVI
i = pixel index
$NDVI\,EM_{non-veg}$ = NDVI endmember non-vegetated
$NDVI\,EM_{veg}$ = NDVI endmember fully vegetated.

NDVI values for the non-vegetated and fully vegetated case were set to the corresponding endmember (Non-vegetated and fully vegetated EM) NDVI values, as extracted for the unmixing approach (see Table 1).

16

In Figure 11 and Figure 12 scatterplots between MEDOKADS NDVI (original and scaled) and GVF are shown for selected decades of the year 2001 for the whole Iberian Peninsula.

For obvious reasons (NDVI does not exceed 0.7), the range of original NDVI values is much lower as the GVF range, as seen in Figure 11. When the NDVI is scaled (Figure 12) to the same range as GVF, the scatterplot is almost arranged around the 1:1 with slightly higher values for GVF. The scatter cloud has especially low dispersions in summer. Well visible is the lower offset in summer time. This should be due to the changes of vertical vegetation density and is shown in more detailed way for the specific test sites in Figure 17 - Figure 21.
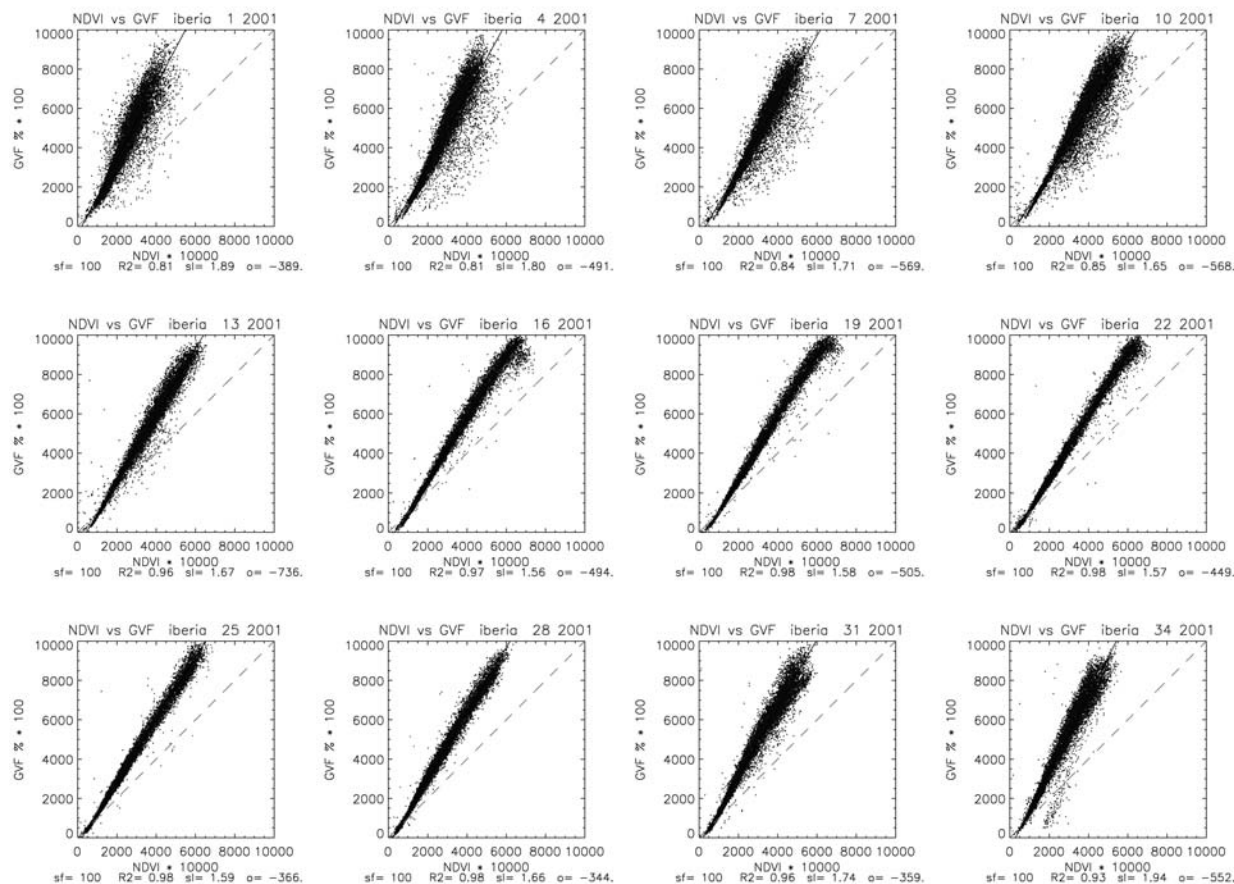

Figure 11 : Comparison MEDOKADS NDVI (x-axis) vs. MEDOKADS GVF (y-axis) for 12 decades of the year 2001 (whole Iberian Peninsula). The continuous line indicates the correlation between both datasets, while the dashed line stands for the 1:1 relationship. Coefficient of determination (R^2), slope (sl) and offset (o) of the regression line are indicated.
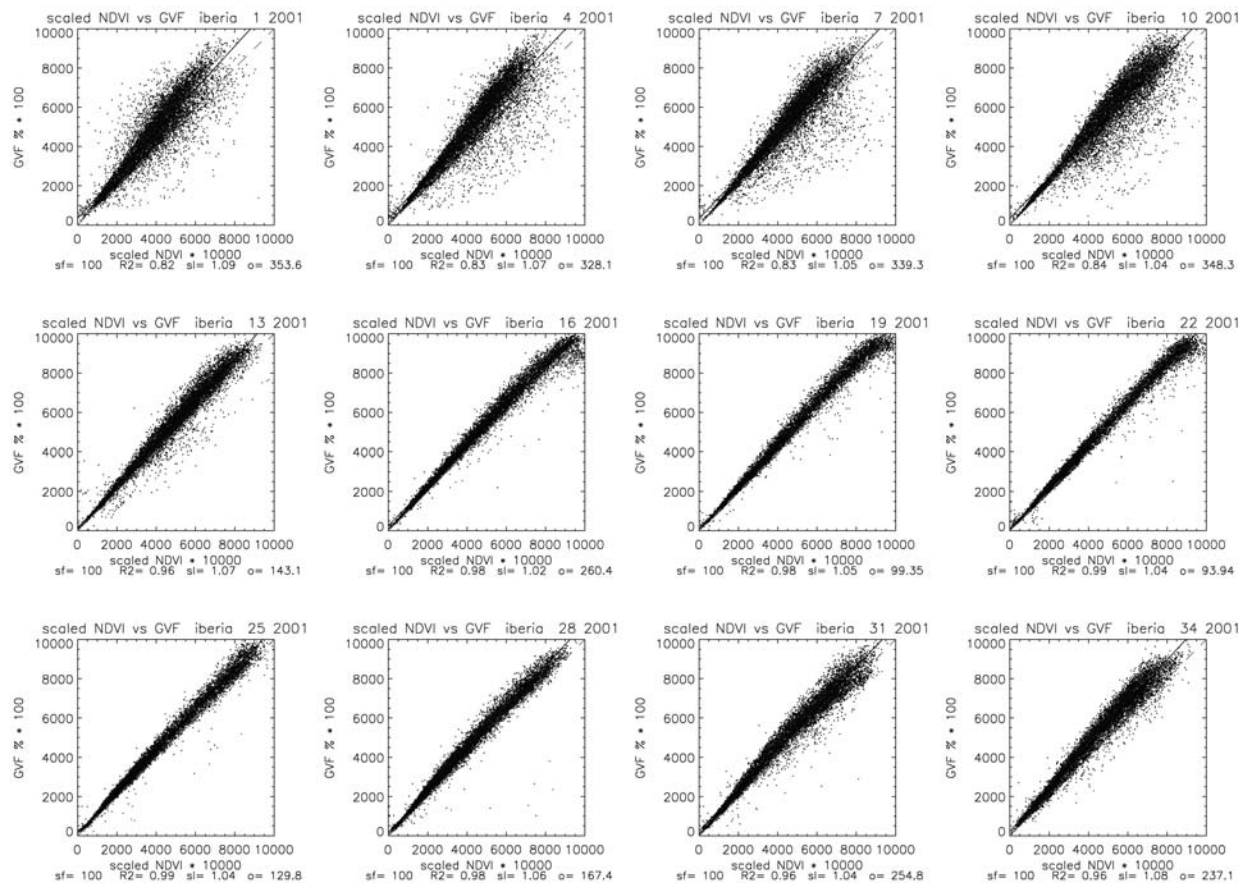
Figure 12 : Comparison MEDOKADS scaled NDVI (x-axis) vs. MEDOKADS GVF (y-axis) for 12 decades of the year 2001 (whole Iberian Peninsula). The continuous line indicates the correlation between both datasets, while the dashed line stands for the 1:1 relationship. Coefficient of determination (R^2), slope (sl) and offset (o) of the regression line are indicated.
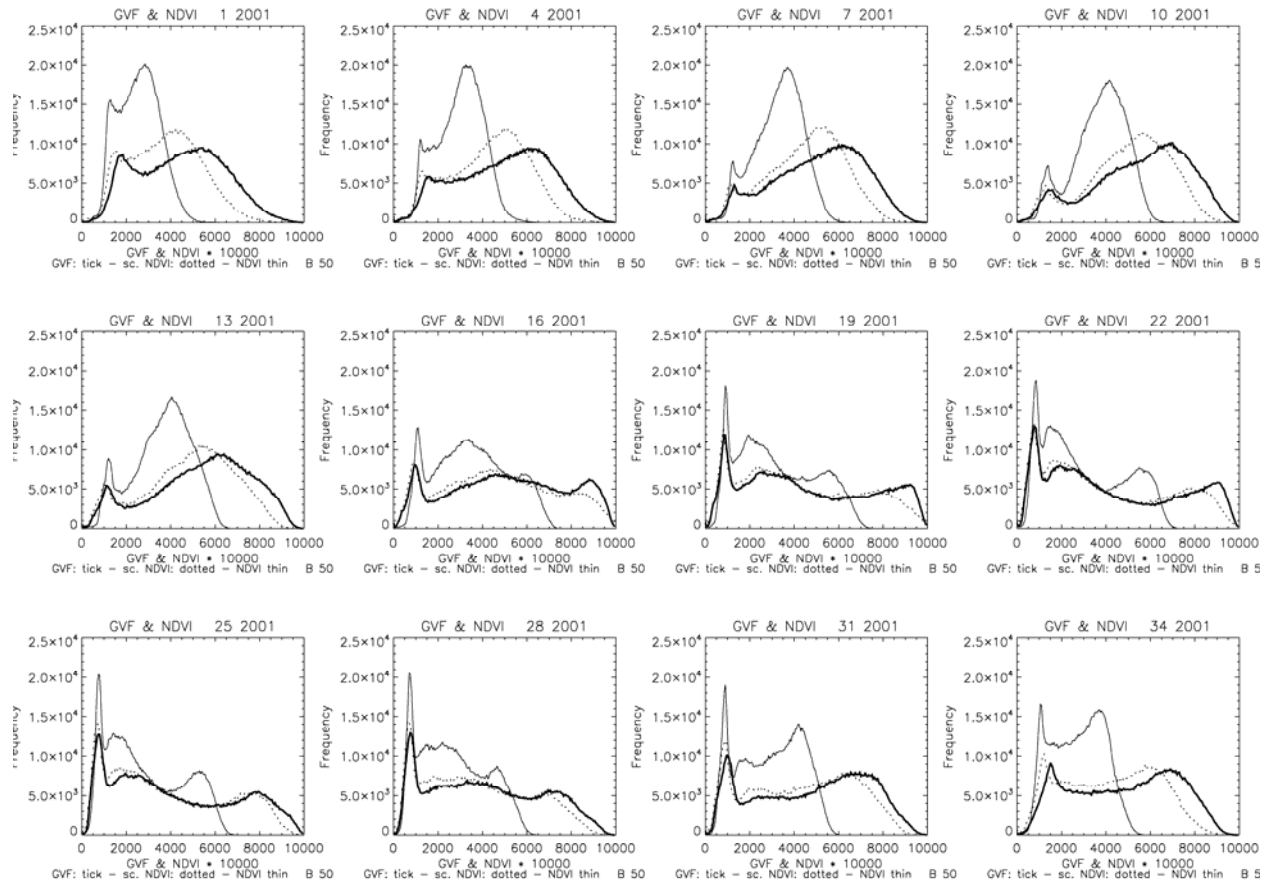
Figure 13 : Histogram comparison between GVF (thick line) and the scaled NDVI (dotted line) and the NDVI (thin line) for 12 decades of the year 2001. The area covers the Iberian Peninsula.

The difference between the GVF and the scaled NDVI becomes more evident when looking at the histograms (Figure 13). This reveals that the overall shape of the histogram is maintained by GVF, but reaches higher values especially during winter when the cold abundance increases.

Results for test sites

Selected test sites for comparison between scaled NDVI and GVF are shown in Figure 14. A description of the test sites is given in Table 2. Two sites with predominantly agricultural land use were chosen in Spain (Valladolid, Cuenca). A test site with broadleaved forest is located in the North of Italy (Pistoia). Furthermore a scarcely vegetated area in Spain (Almeria) and a desert area in Tunisia were selected.

The GVF follows closely the seasonal run of the scaled NDVI in all test sites (see Figure 15). The GVF is generally slightly higher (not for Tunisian desert), which should be due to the normalisation of GVF, as reported above (see Eq. 7).
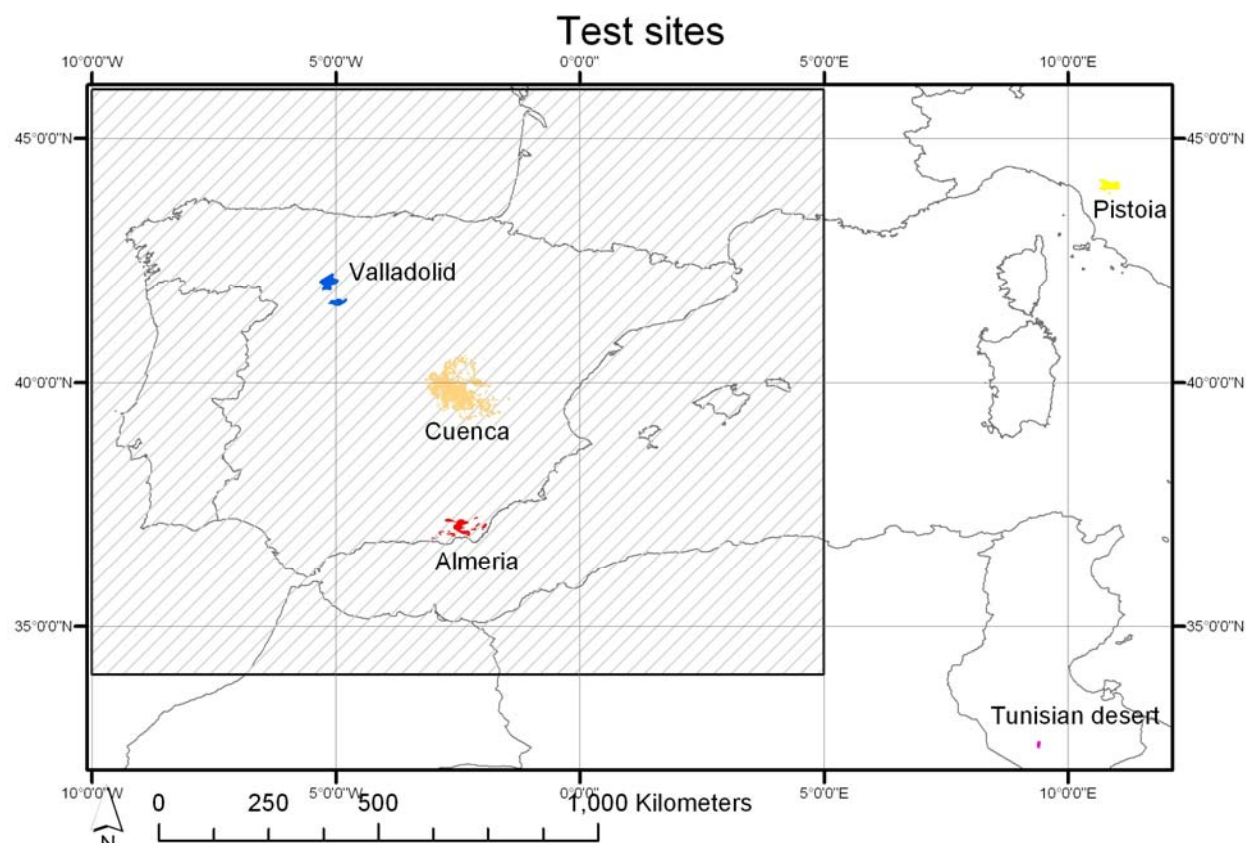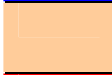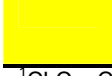
Figure 14 : Specific test sites for data comparison. The subset of the "Iberian Peninsula" (including also parts of North Africa) is depicted as hatched rectangle.

**Table 2 : The specific test sites (see also Figure 14):**

Colour	Name	Description	n (pixels)
	Valladolid	A manually delineated area around Valladolid, predominated by agricultural land use, disposing of a high degree of seasonal vegetation dynamic.	1 167
	Cuenca	CLC[1] class 12 ('non-irrigated arable land'), limited to the province of Cuenca and to pixels, that contained a minimum of 80 % of the respective land cover.	3 142
	Almeria	A manually delineated area around Almeria, predominated by scarcely vegetated land cover.	997
	Tunisian desert	A manually delineated area in the Tunisian desert predominated by the GLC[2] class 'sandy dunes'.	103
	Pistoia	CLC class 23 (broadleaved forest), limited to the Italian province of Pistoia and to pixels, that contained a minimum of 70 % of the respective land cover	315

[1]CLC – Corine Land Cover 2000 (EEA, 2006)
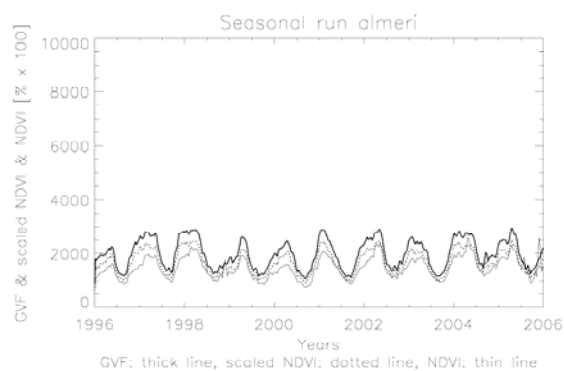[2]GLC – Global Land Cover 2000 http://www-gvm.jrc.it/glc2000
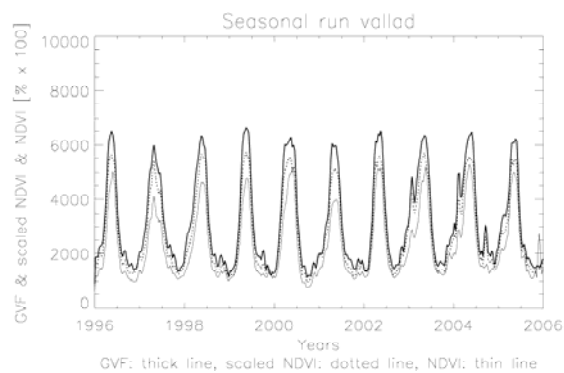
a)
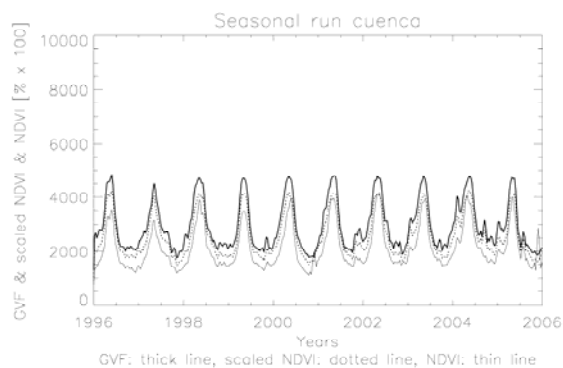
b)

c)
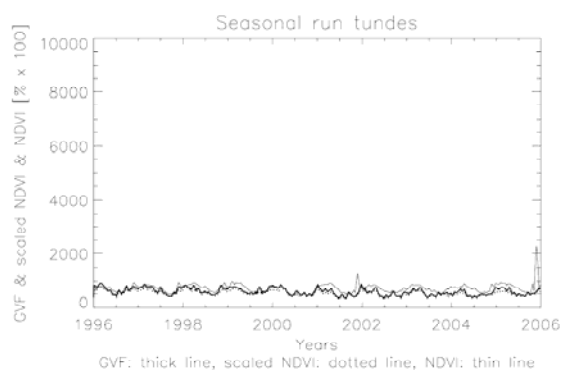
d)
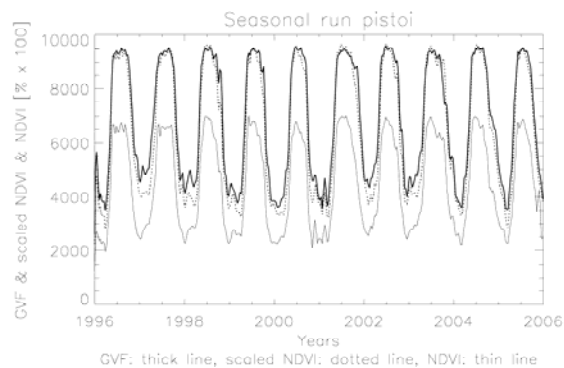
e)

Figure 15 : Temporal profile of scaled NDVI and GVF for test sites in the Mediterranean: a) Valladolid, b) Cuenca c) Almeria, d) Tunisian desert and e) Pistoia.
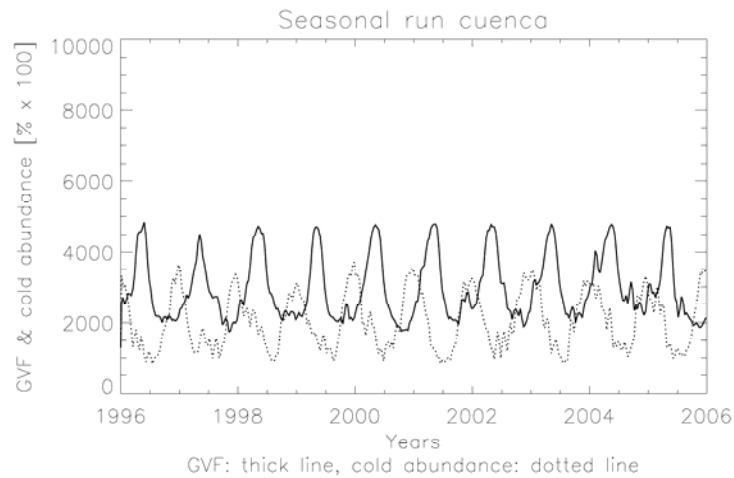
Figure 16 : Green vegetation fraction [% * 100] and cold abundance for test site Cuenca.

The seasonal run of GVF and cold abundance is depicted in Figure 16. The peaks of the cold abundance are most pronounced in the cold season (end/beginning of the year). In comparison to the scaled NDVI the GVF (which re-distributes the cold abundance proportionally to the remaining vegetation abundance and soil abundance) is therefore generally higher during the cold season (see Figure 15). The higher values of GVF on top of the growing peaks instead might be due to the proportional re-distribution of the cold EM, which is favouring GVF for a cold abundance assignment around the growing cycle peak.

Scatter diagrams of scaled NDVI versus GVF for selected decades for each test side are shown in Figure 17 - Figure 21. For both agricultural test sites Valladolid and Cuenca, GVF tends to be slightly higher, the difference increasing with higher values.

Figure 17 : Scatter diagrams (GVF vs. scaled NDVI) for the test site Valladolid for selected decades of the year 2001. Coefficient of determination (R^2), slope (sl) and offset (o) of the regression line are indicated.
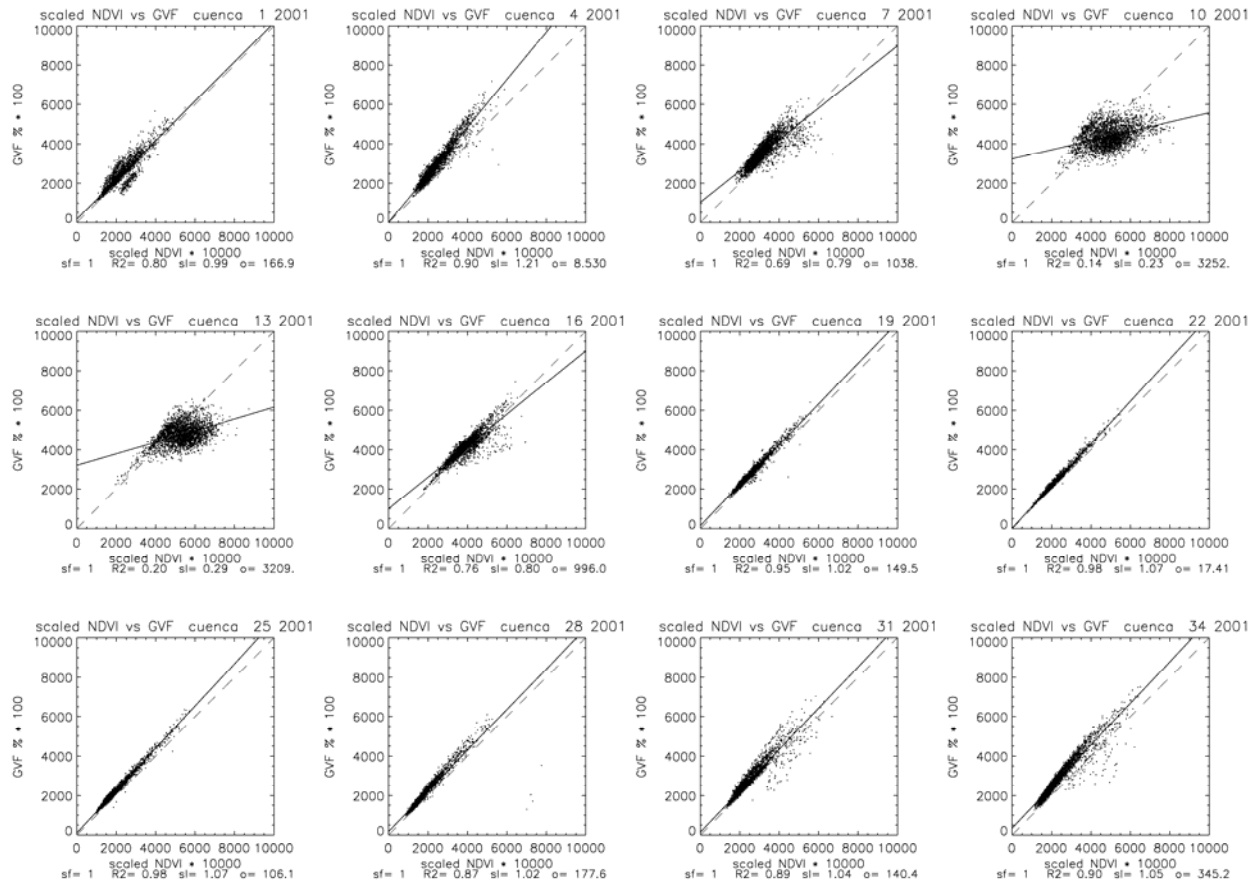
Figure 18 : Scatter diagrams (GVF vs. scaled NDVI) for the test site Cuenca for selected decades of the year 2001. Coefficient of determination (R^2), slope (sl) and offset (o) of the regression line are indicated.
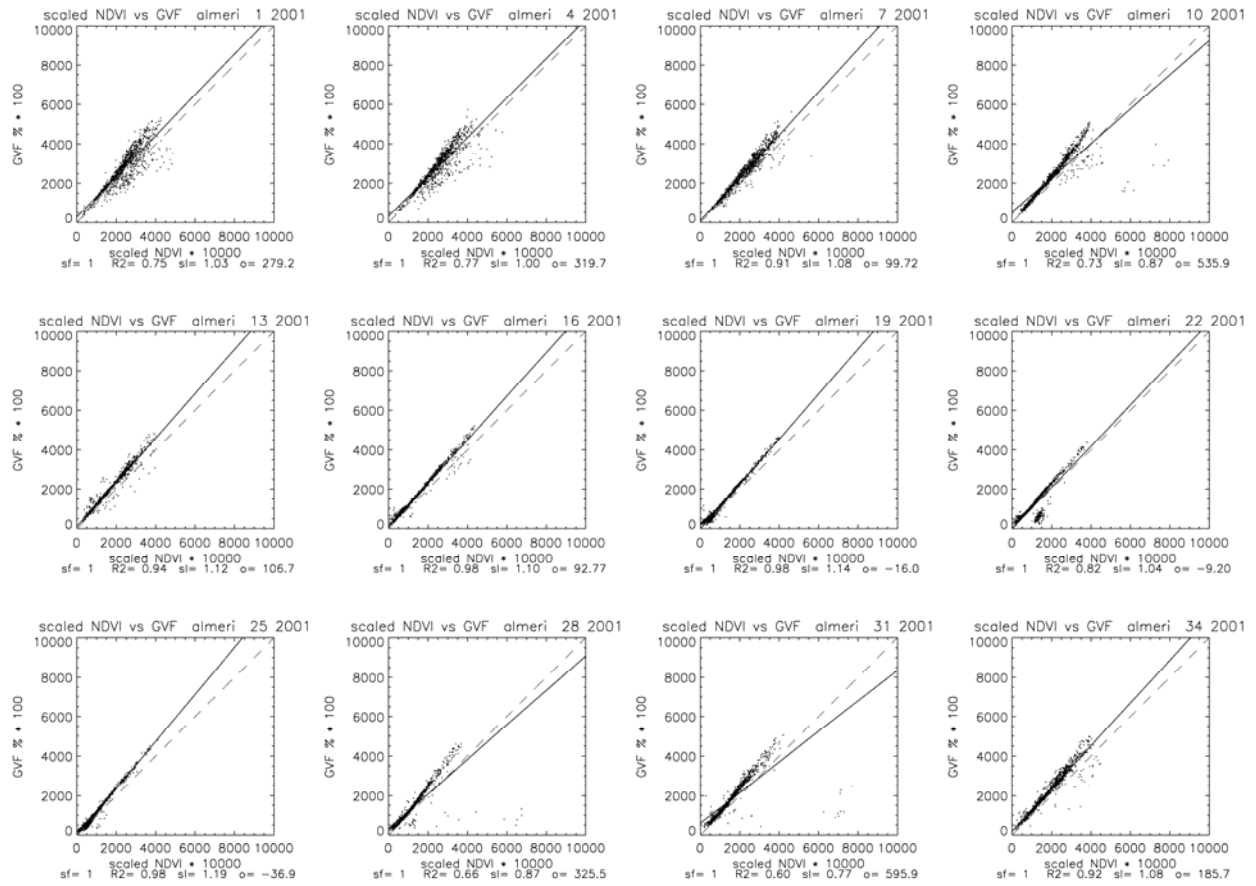
Figure 19 : Scatter diagrams (GVF vs. scaled NDVI) for the test site Almeria for selected decades of the year 2001. Coefficient of determination (R^2), slope (sl) and offset (o) of the regression line are indicated.

For the scarcely vegetated test site Almeria GVF and scaled NDVI show a good fit in the low range. A notable offset with higher GVF values can be observed for values above 0.15 – 0.20.
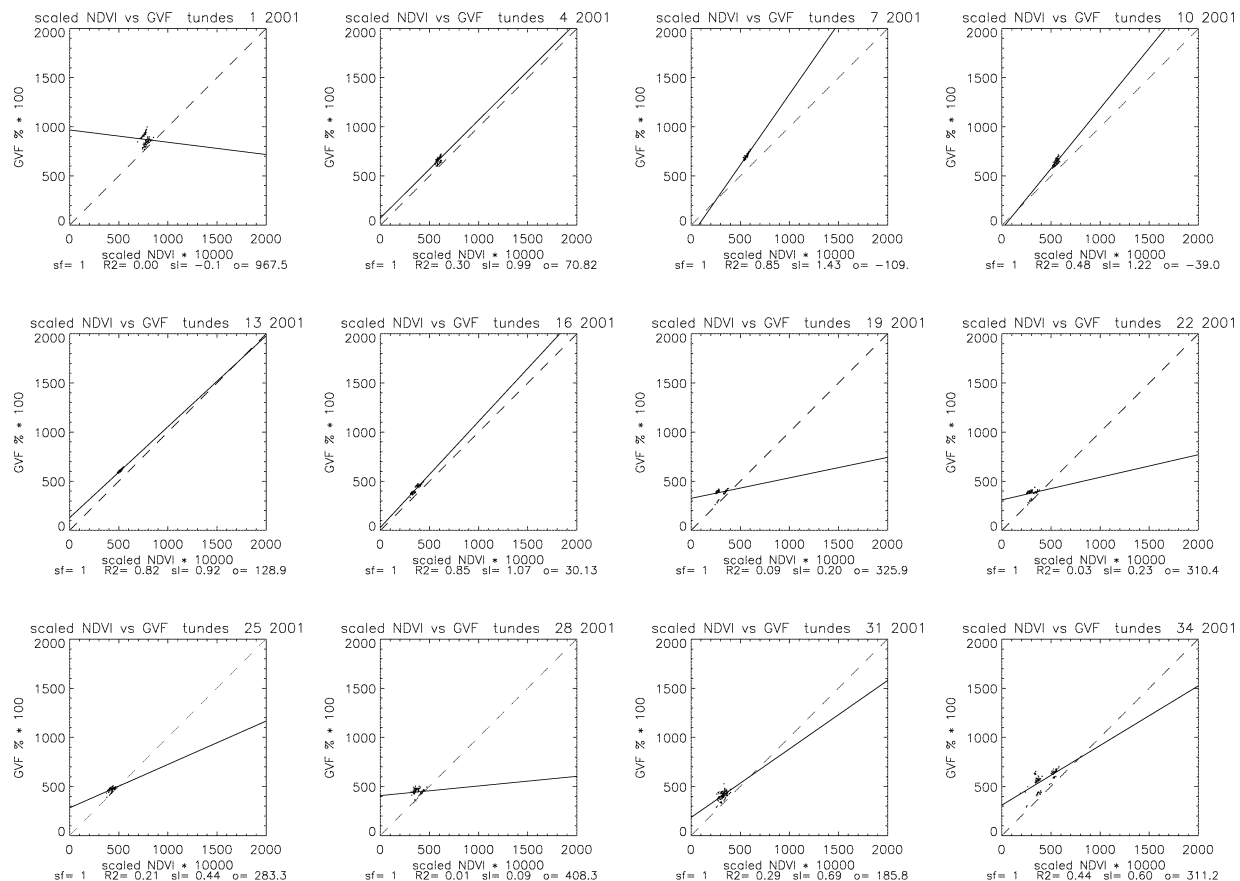
Figure 20 : Scatter diagrams (GVF vs. scaled NDVI) for the test site Tunisian desert for selected decades of the year 2001. Coefficient of determination (R^2), slope (sl) and offset (o) of the regression line are indicated.

The difference between GVF and scaled NDVI for the test site in the Tunisian desert is low, for most decades there could be observed a slightly higher GVF of approx. 0.01 units.
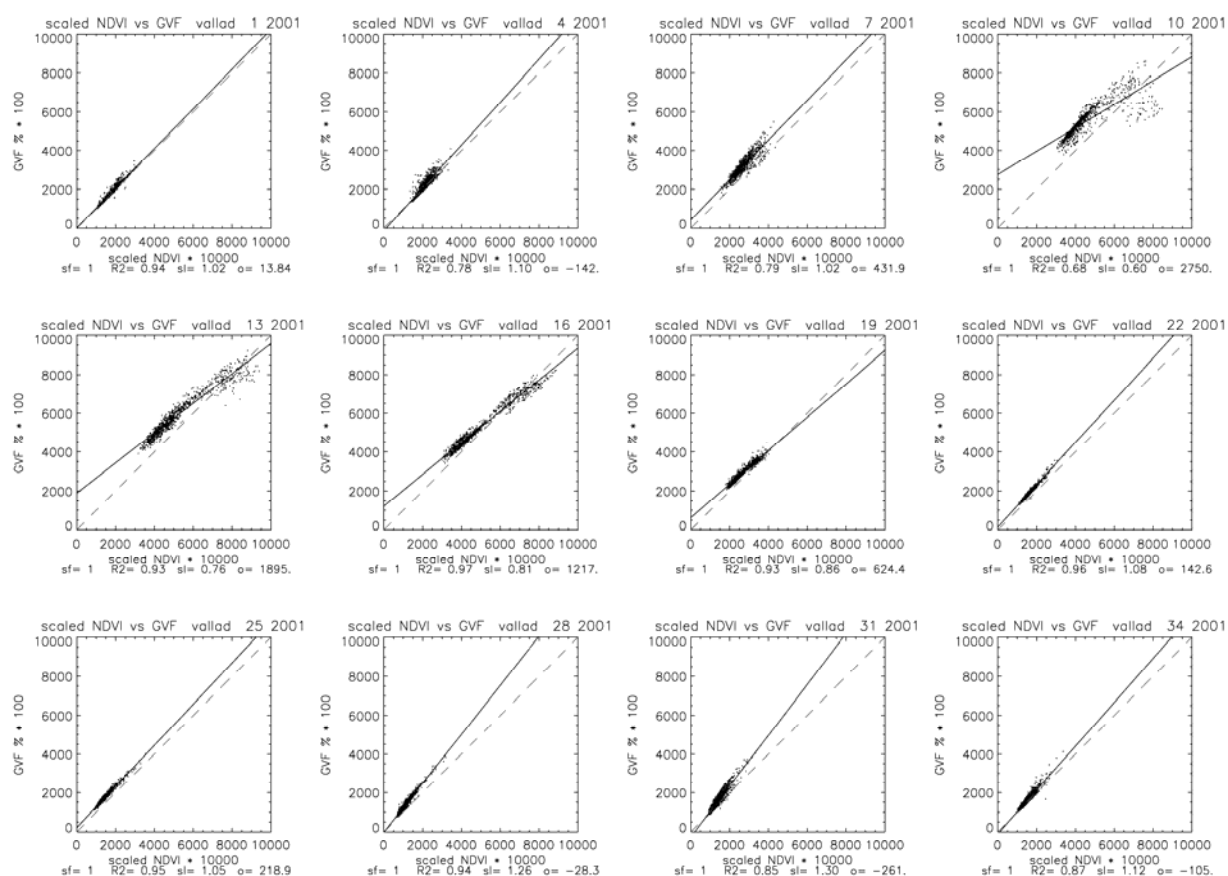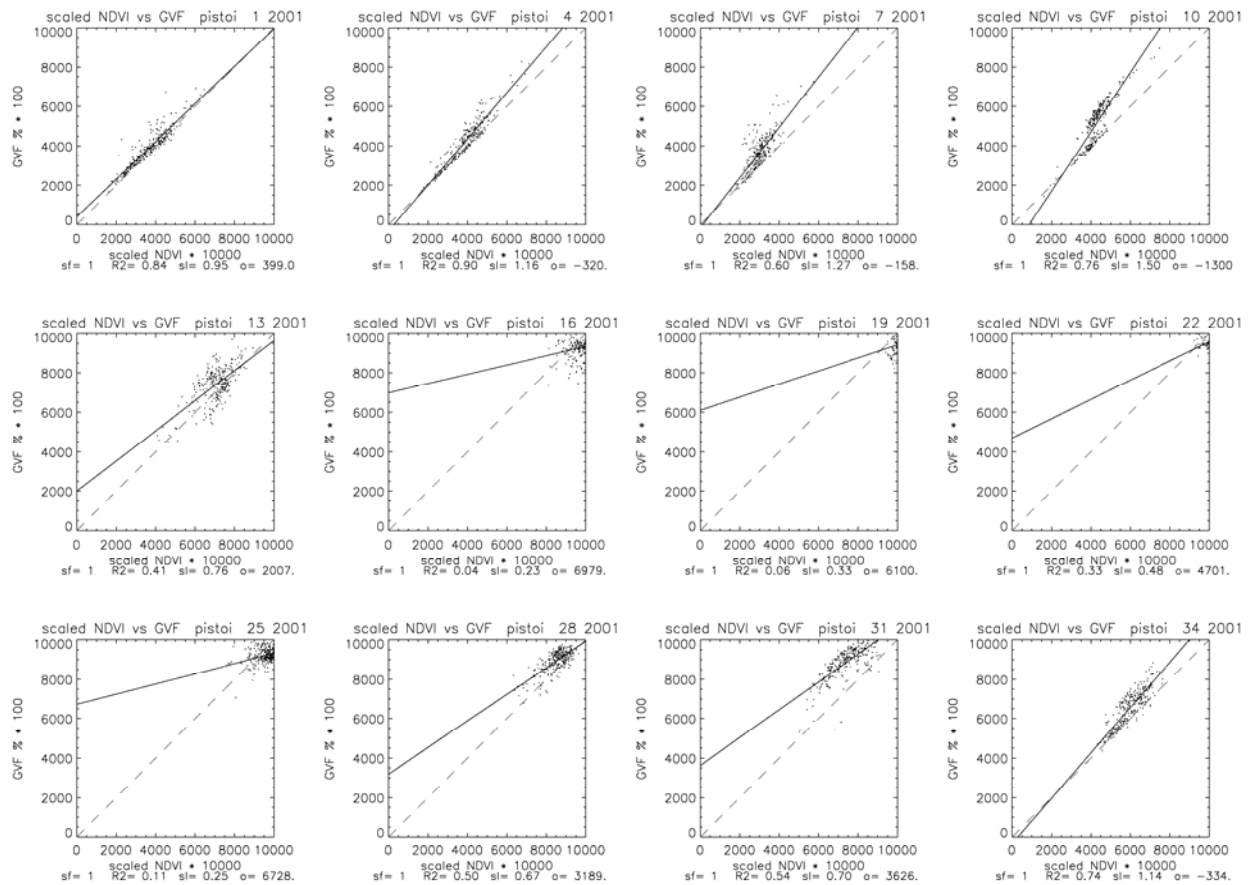
Figure 21: Scatter diagrams (GVF vs. scaled NDVI) for the test site Pistoia for selected decades of the year 2001. Coefficient of determination (R^2), slope (sl) and offset (o) of the regression line are indicated.

As for a broadleaved deciduous forest (Figure 21), the GVF/scaled NDVI scatter moves along the 1:1 line when onset and senescence of the growing cycle occur. The sideward movement (offset) is due to changes of the vertical vegetation density (LAI), as this was shown by other authors (Gutman & Ignatov, 1998; Myneni et al., 1992).

Effect of the cold abundance on GVF

Does the cold abundance contribute to an improvement of the GVF and if so, to which extent? As reported earlier (see introduction), several effects may lead to a wrong NDVI. Amongst them, atmospheric effects, which are not eliminated by the maximum value compositing algorithm, play a major role. Generally, clouds and poor atmospheric conditions depress NDVI values (Chen et al., 2004). In the case of GVF, this effect should be attenuated by the normalization, when the cold abundance (if being between 0 and 30 %) is re-distributed to the remaining fractions.

GVF and NDVI for cases of large cold fraction (20-30 %)
First decade of May 1989 - 2005
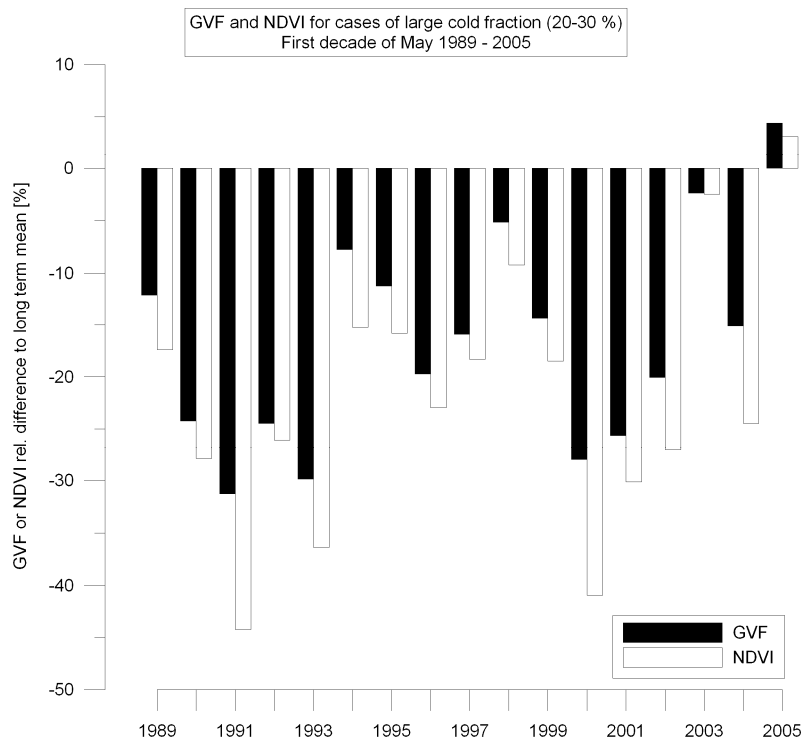
Figure 22 : Deviation of unfiltered GVF and NDVI to their long term mean for pixels of a (unfiltered) cold abundance between 20 – 30 %. Only 'stable' pixels (no land use change supposed) were used. Data refers the first decade of May 1989 – 2005 for the Iberian Peninsula.

The effect was tested for the subset of the Iberian Peninsula for the first decade of May of all years 1989-2005. Out of this subset, only pixels of supposed 'stable' land use types were used. Supposed 'stable' pixels were extracted from unfiltered NDVI data for each decade and pixel, considering the deviation to the long term median. These represented mainly forests and sclerophyllous vegetation, while urban areas and agricultural land use types were excluded. As Figure 22 shows, both GVF and NDVI show negative deviations from their long term mean in the case of a high cold abundance of 20-30 % (except for the year 2005). However, the negative deviations are clearly larger for the NDVI, the difference between GVF and NDVI ranging between -0.1 and -13.0 % percentage points, in average

over all years 1989-2005 amounting to -5.4 percentage points. It should be noted that the degree of compensation of poor atmospheric conditions via cold abundance is depending on the relation of vegetation and soil abundance: A strong compensation is theoretically possible in the case of abundances closed to 100 %, where the cold abundance has a strong absolute compensation effect with normalisation (see Eq. 7). In the case of equal values for soil and vegetation abundance the cold abundance is distributed equally and has hence a minor impact on the absolute value of the single fraction.

Keeping in mind, that the pixels used in Figure 22 are supposed to be stable (no land use change, no seasonal change), it indicates, that the GVF is much closer to stability than the NDVI.

Data quality

As Eidenshink (2008) reports for a similar data set there are three primary factors that affect the data quality of NOAA AVHRR composite data sets: Cloud contamination, aerosol contamination and the orbital drift. Cloud contamination is considered first by application of a cloud mask and second by normalisation of the data by the cold abundance. There is no correction for aerosol contamination applied. The largest effect of aerosol contamination occurs during volcanic eruptions and major wildfire outbreaks. There has been one major volcanic eruption in 1991 (Mt. Pinatubo). Mt. Pinatubo eruption had the most significant effect on the stratospheric aerosol in the equatorial region of the world. As reported by the author, the impact in the northern hemisphere was relatively smaller. The third factor is satellite orbital drift. Despite SZA correction and normalisation of surface temperature there were observed relatively low values for the year 1999 and 2000, which are due to the orbital drift of NOAA-14 (Figure 23) and related negative effects (BRDF effects and atmosphere induced effects). The correction for SZA, as it was performed, was not sufficient, as this is shown also in Figure 5. At launch the typical time of day for the NOAA-AVHRR afternoon observation is 1:30 pm local solar

time, in 2000, the time of observation of NOAA-14 drifted past 5:00 local solar time. This has to be considered especially for long-term observations or analysis (e.g. trend analysis). Eidenshink (2008) e.g., did not consider the year 2000 data for long term means.

To get a better understanding of the data around the critical year 2000, a comparison of three standardized time series ranging from 1998 – 2004 were carried out and displayed in Figure 23. The first time series comprised the MEDOKADS NDVI (not scaled), the second one represents the results of unmixing, i.e. the GVF time series. The FAPAR data (Gobron et al. (2000); http://fapar.jrc.it/) is shown as a reference. In order to avoid effects from specific land cover types, the test was applied to the whole Iberian Peninsula, using pixels with no land cover change. To detect the stable areas, CLC 1990 and CLC 2000 was used (EEA, 2004). Also, the data was aggregated to yearly mean values to reduce effects of seasonality. The standardization of the data was carried out as z-score normalisation (also referred to as autoscaling or zero-mean normalisation). Here, the values for an attribute U are normalized based on the local mean ū (1998 – 2004) and the local standard deviation s of U.

$$u' = \frac{U - \bar{u}}{s} \tag{9}$$

Figure 23 shows NDVI and GVF with a strong depression in the year 2000, while FAPAR, being based on a different sensor (SeaWIFS), is relatively stable. NDVI and GVF exhibit an almost identical run (years 1999, 2001 and 2002), GVF being closer to FAPAR in 1998, 2000, 2003 and 2004. This comparison, however, is indicative, note, that for a proper comparison a longer time span would be needed.
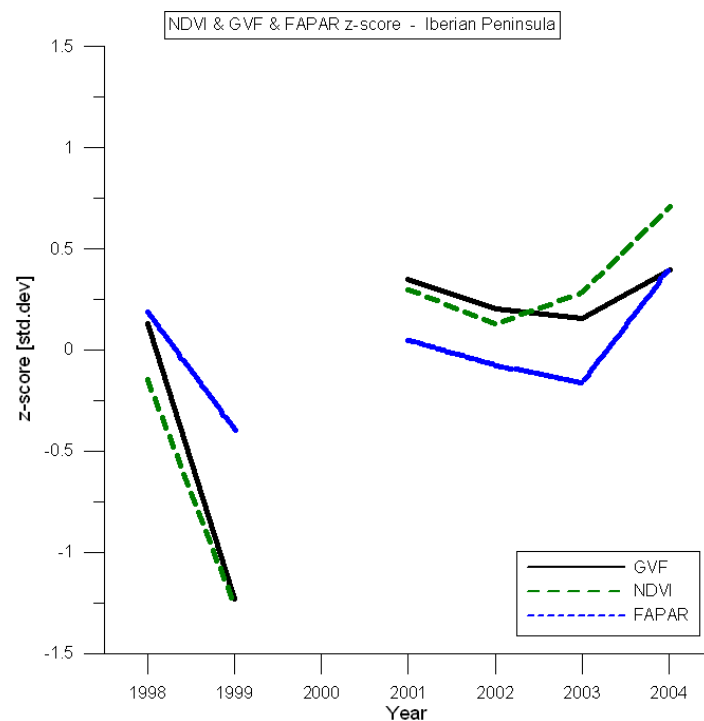

Figure 23 : z-score comparison for GVF, NDVI and FAPAR, averaged for the Iberian Peninsula. Only pixels with stable land cover were used. Z-score calculation was computed over the years 1998-2004 only.

Comparison with independent data

GVF was compared with independently derived vegetation cover (fCover) estimates for VALERI network[2] test sites. Within VALERI, a methodology has been developed to derive biophysical parameters at spatial resolution of large swath satellites from ground measurements. Each field measurement site comprises a flat area of 3km x 3 km, which is relatively homogenous. Sampling is done for selected elementary units (20 m x 20 m) that represent the variability observed within the whole site. Gap fraction (which is the bare soil percentage seen from a given viewing angle equals the 1- % cover at nadir) measurements were performed either with LAI2000 Plant Canopy Analyser (Li-Cor) or hemispherical photographs. Accordingly, fCover was defined as the percentage of soil covered by vegetation between 0 º and 7º view zenith angle In order to upscale the ground measurements to corresponding high resolution SPOT imagery empirical transfer functions and co-kriging techniques were applied. Detailed description of sites, field measurements and retrieval of vegetation cover from SPOT HRV is given for each site on the VALERI network website. The sites vary in land cover type and in the timing of ground truth measurements / SPOT HRV data acquisition (see Table 3).

The RMSE (cross-validated) for transfer functions from ground measurements to SPOT data was given in the range from 0.1 – 0.22 for the different sites.

Table 3 : Test sites of VALERI network for comparison with GVF values.

VALERI site	*Abbreviation*	*Land cover*	*SPOT image acquisition*	*Decade from GVF time series*
Nezer	NEa	pine forest	20/07/2000 & 01/08/2000	21/2000
	NEb		02/04/2001	10/2001
	NEc		20/06/2001	17/2001
	NEd		21/04/2002	12/2001
Haouz	HA	crops	04/03/2003 & 25/03/2003	08/2003
Les Alpilles	AP	crops	20/07/2002	20/2002
Plan-de-Dieu	PD	crops	29/06/2004	18/2004
Puéchabon	PU	Mediterranean forest (oaks)	12/06/2001	17/2001
Sud-Ouest	SU	crops	20/07/2002	20/2002
Le Larzac	LA	grassland	12/07/2002	20/2002
Barrax	BA	crops	03/07/2003	19/2003

---

[2] http://www.avignon.inra.fr/valeri/

a)

b)

Figure 24 : Comparison of (a) GVF and (b) approximated fractional vegetation cover (see eq. 11) with vegetation cover derived by high resolution imagery stemming from SPOT HRV for VALERI test sites. Values are averaged over 3 km x 3 km. Error bars give standard deviation. For abbreviations see Table 3.

For the comparison SPOT HRV fCover of 20 m resolution was aggregated to 1 km resolution. Mean values and standard deviation of fCover and GVF, as shown in Figure 24, were derived from a matrix of 3 x 3 pixels from both datasets.

Certainly, different geometrical issues have to be considered when comparing different products: the geo-location accuracy, the point spread function (PSF) and the projection system. As the VALERI network provides only a subset of the SPOT HRV data for each test site (in most cases 151 x 151 pixels) a co-registration of GVF and Spot HRV data was not feasible.

The revealed relation between GVF and fCover is linear. GVF values result in average 15 % higher. Differences in SPOT fCover estimates between June 2000 (NEa) and July 2001(NEc) for test site Nezer, which do not occur in the GVF, may be explained with problems during the field measurements after a storm event in 1999 and a modified sampling protocol in 2001 as reported by Guyon (2000, 2001).
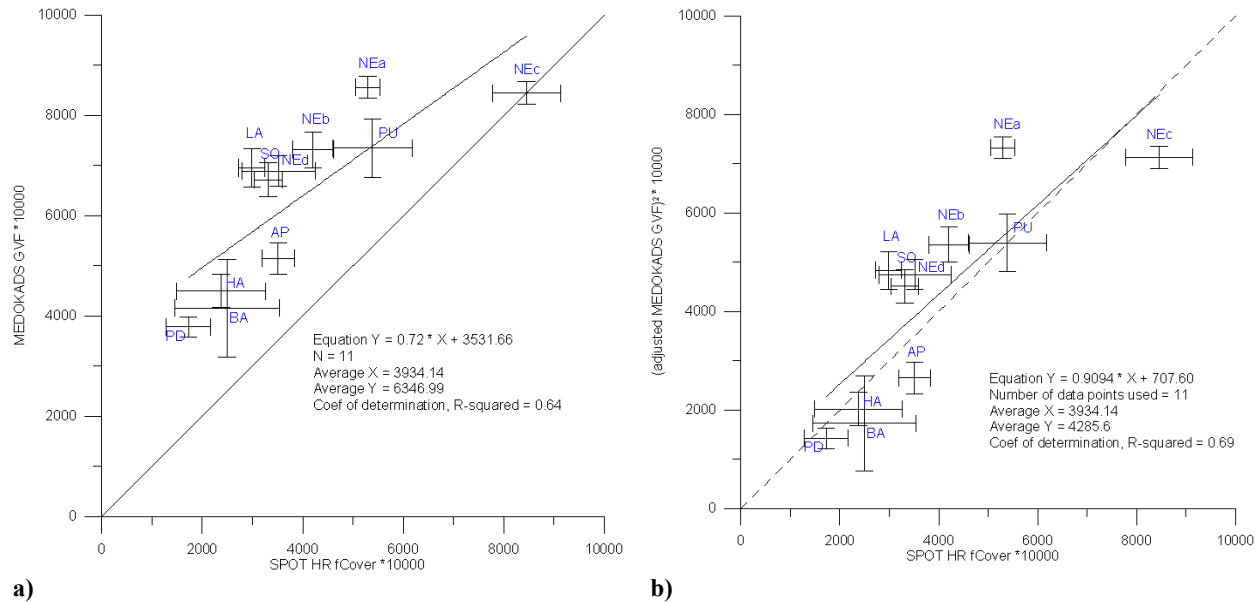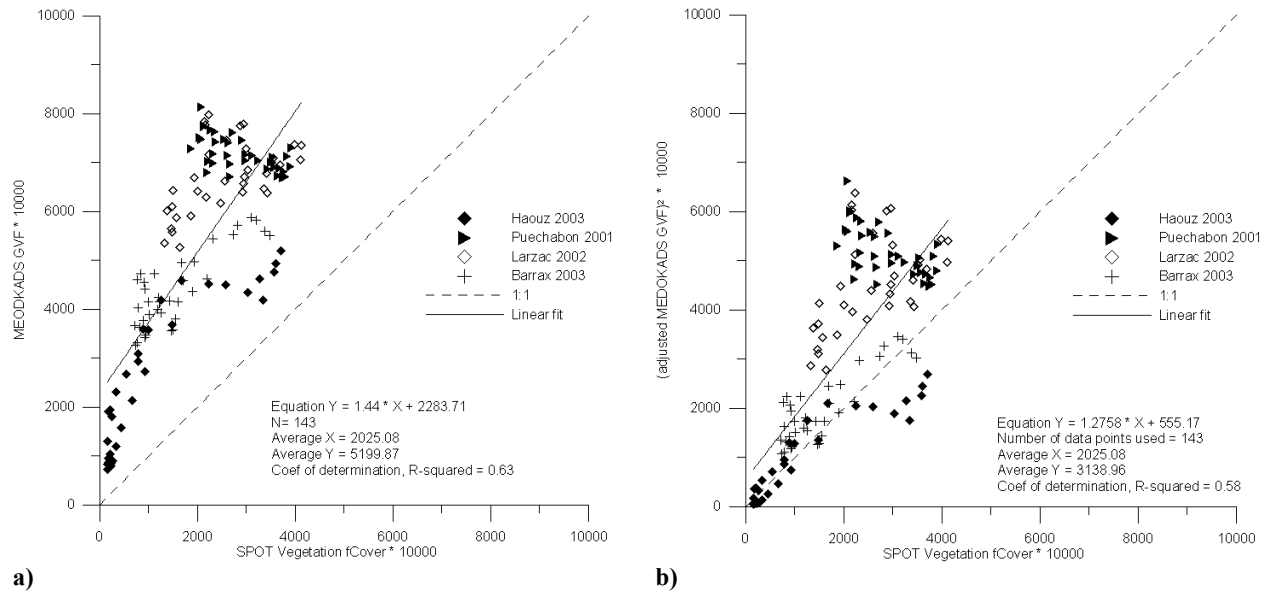
31

Figure 25 : Comparison of GVF (a) and approximated fractional vegetation cover (b, see eq. 11) with vegetation cover derived from SPOT VEGETATION for VALERI test sites Values are averaged over 3 km x 3 km.

For selected VALERI sites with different land cover types, GVF was compared with the CYCLOPES (Carbon cYcle and Change in Land Observational Products from an Ensemble of Satellites) fCover product. The CYCLOPES algorithm for the derivation of biophysical variables (LAI, fapar and fCover) from SPOT VEGETATION is based on training of neural networks over SAIL + PROSPECT radiative transfer model simulations for each biophysical variable (Baret et al., 2007). Inputs of the networks are made of the median value of the sun zenith angle observed during the compositing period and normalized top of canopy nadir reflectance in three VEGETATION bands 2 (645 nm, $\Delta\lambda$ 70 nm), 3 (835 nm, $\Delta\lambda$ 70 nm), and Short Wave Infrared (1165, $\Delta\lambda$ 170 nm). FCover refers only to the green vegetation elements. Products and detailed documentation are available at http://postel.mediasfrance.org. For the comparison CYCLOPES product version 3.1 Level 3 B has been used. Figure 25 shows the scatter diagram of GVF and CYCLOPES fCover for 36 decades for each test site (including different years). Values for each site were averaged over 3 km x 3 km for both datasets. Again, the relationship between both estimates is linear with higher values for the GVF. A low maximum value (0.6) for the CYCLOPES fCover product is reported in the CYCLOPES product information (Medias France, 2006). CYCLOPES fCover values for the site Puechabon (Mediterranean oak forest dominated by *Quercus ilex*) are lower than 0.4 throughout the year in contrast to GVF with values at about 0.7. The vegetation cover estimate from high resolution SPOT from June 2001 indicates a 'true cover' between values from both data sets. Furthermore CYCLOPES fCover for this site shows a seasonal variation of vegetation cover which can not be observed in the GVF (Figure 26 a). The SPOT VEGETATION NDVI shows no seasonal variation in agreement with GVF.

a)   b)
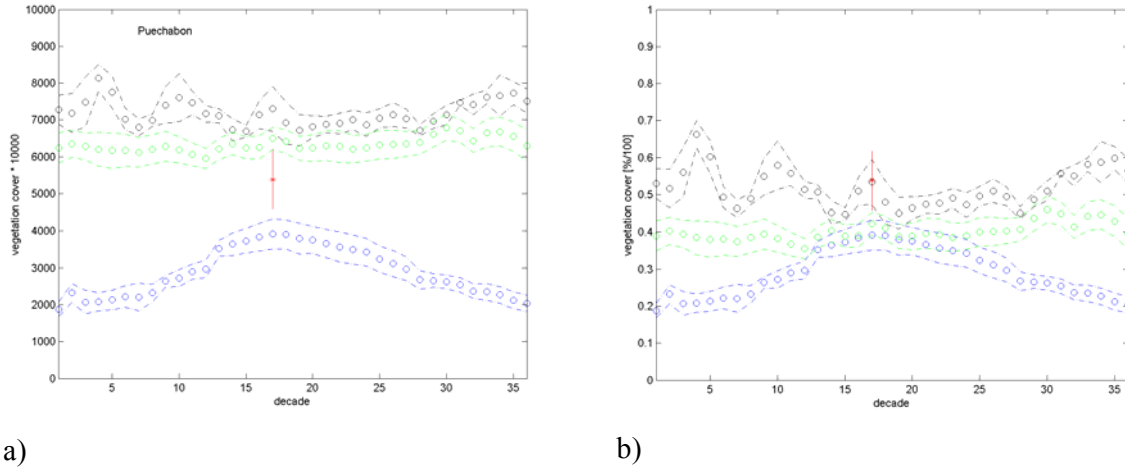
Figure 26 : Temporal profile of (a) GVF (black o), SPOT VEGETATION fCover (blue o) and SPOT NDVI (green o), (b) fractional cover from GVF (black o), SPOT VEGETATION fCover (blue o) and fractional cover from SPOT NDVI (green o) for Puechabon in 2001. Values are averaged over 3 km x 3 km. Standard deviation is indicated (--). FCover estimate from the high resolution SPOT data is given (average 3 km x 3 km) in red (*) with standard deviation (-). For the derivation of fractional cover from GVF and SPOT NDVI see eq. 11 and eq. 10.

The results shown in Figure 24 a, Figure 25 a and Figure 26 a clearly indicate that our obtained GVF values are higher than CYCLOPES fCover. A literature research revealed that there was found in several cases a relation between a scaled NDVI and fractional vegetation cover. The close relation between GVF and the scaled NDVI (almost 1:1) allowed an approximate calculation of fractional vegetation cover, as outlined below.

Choudhury et al. (1994) and Gillies & Carlson (1995) independently obtained an identical square root relation between a scaled NDVI and fractional vegetation cover, which was later confirmed by findings of Carlson & Ripley (1997) (see equation 10). Fractional vegetation cover is defined as green vegetation cover per unit horizontal surface area.

$$Fractional\ vegetation\ cover \quad \approx \left(NDVI_{scaled}\right)^2 \tag{10}$$

Our obtained GVF was highly correlated to the scaled NDVI, as can be seen from Figure 12. The relation was almost 1:1, with slightly higher values for GVF, especially in the higher ranges. Assuming a direct 1:1 linear relation between the scaled NDVI and GVF, the square of the 'corrected' GVF should be a real measure of fractional vegetation cover, comparable to the CYCLOPES fCover.

$$Fractional\ vegetation\ cover \quad \approx \left(GVF\right)^2 \tag{11}$$

A comparison of calculated fractional vegetation cover according to equation 11 on one side and SPOT HRV fCover and CYCLOPES fCover on the other side is shown in Figure 24 b and Figure 25 b.

Discussion

Advantages of this Unmixing approach

NOAA AVHRR is the longest available remote sensing time series. It is known that this satellite system is affected by some undesirable properties, e.g. high oscillations due to a bad signal to noise ratio or weak geometrical accuracy. Unlike a simple NDVI, which uses 2 channels only, the Unmixing is based on 4 NOAA AVHRR channels and built on a physically based relationship between ratios or combinations of these channels. Certainly, Unmixing is depending on the base data as well as a vegetation index, but mitigates the risk of erroneous data propagation due to its multi-dimensional approach.

Another advantage of the Unmixing has to be regarded the fact, that this technique delivers three basic outcomes, a vegetation abundance, a bare soil abundance and a cold abundance. All of them can be utilized per se and present subpixel information. For obvious reasons the main focus of our data derivation was the vegetation abundance, which we normalised (see Eq. 7) and hence corrected for the existence of the cold abundance (fourth outcome). The normalised vegetation fraction (GVF) represents a refined product for vegetation estimates, corrected for effects that lower the surface temperature of the surface, e.g. effects related to altitude and exposition, temperature variations due to soil moisture, variable evapo(transpi)ration and remaining atmospheric effects and cloud artifacts. Moreover, the position in the Unmixing triangle allows conclusions about occurring evaporation/transpiration potential.

While direct NDVI transferability of different sensors is critical, the GVF represents a better standardized and hence comparable product, which could be derived from any sensor delivering the necessary input variables NDVI and Ts. This comparability was shown for Landsat TM derived GVF and NOAA AVHRR derived GVF for the Ayora region in Spain by Stellmes et al. (2005). The relationship between both data sets was linear, almost 1:1.

The comparison with independently derived fractional vegetation cover shows clearly, that GVF contains considerable volumetric vegetation information, similar as NDVI does. Although the name Green Vegetation Fraction might be misleading in this sense, it was kept for historical reasons. However, the term 'normalized vegetation abundance' would reflect better the real properties of the parameter. GVF data is higher in comparison to CYCLOPES fCover although these validation data might be too low in general, as stated by the authors themselves. GVF may be considered an improved vegetation index which is similar to NDVI, as for the volumetric vegetation information. Most important improvements of GVF in comparison to NDVI are the atmospheric disturbance mitigation and the widening of range (scaling). Also the derivation of useful by-products from the unmixing process and the enhanced cross-comparability of the data are valuable.
The approximation of a real fractional vegetation cover by squaring GVF leads to close results to the CYCLOPES fCover and confirms this approximation technique reported in literature.

Assumptions and limitations

As reported above, the approach is based on an inverse relationship between NDVI and surface temperature Ts. This inverse relationship is best pronounced during the growing cycle, when some vegetation is on ground and acts as cooling agent. On the contrary, the relationship is not inverted for regions with extreme cold conditions, when vegetation acts as a warming rather than a cooling agent. Hence, this approach is limited to areas of moderate warm or hot temperatures and does not apply, e.g. for high mountainous regions.

Other regions of limited suitability for this approach are wetlands or areas of high moisture content. The presence of surface water biases the relationship NDVI-Ts as the cooling effect does mainly derive from the surface water. These areas, however, are recorded by the system as areas with a high 'cold' abundance and are eventually excluded.

Also, over evergreen forests, without a moisture availability constraint, the Ts-NDVI relation is modified compared to water limited environments. This is often the case in the tropics. At the scale of a decade the slope of the Ts-NDVI relation is positive (Lambin & Ehrlich, 1996). However, this does not apply for the Mediterranean area with its classical dryland areas.

A crucial issue for unmixing is the identification of the endmembers (EM). Since scaling of the data is determined by the EMs, these should be chosen with care. In order to guarantee the comparability of the derived data, windows for the extraction of EMs were kept large. Still, the different climatic conditions for Western and Eastern Europe are attempted to be treated differently by the two chosen windows.

The quality of the derived GVF data set depends considerably on the base MEDOKADS data. Although enormous effort was put into correction of the MEDOKADS base data, there are still deficiencies, as reported earlier e.g. the decline of the year 2000 mainly due to the late overpass of NOAA14 in its late operating period. Even though some problems could be mitigated by empirical approaches, some deficiencies linked to atmospheric effects and illumination effects (BRDF) could not be fully corrected. In comparison to the NDVI, the GVF was generally showing a run closer to the independent data set FAPAR.

An additional factor to consider is the switch from AVHRR/2 to AVHRR/3 instrument, which occurred after the year 2000. The effect of AVHRR/3 is generally a higher NDVI, due to different band widths in the red and infrared wavelength range. The switch can not be easily corrected and was hence not corrected at all for MEDOKADS. The effect is expected to be mitigated by (decadal) Unmixing. A proper demonstration of positive Unmixing effects on the 'instrumental switch' is difficult since the 'orbital drift' effect is overlaid.

Conclusions

Main outcome of this project is a post-processed and validated data base of Green Vegetation Fraction for the period 1989-2005, covering the Mediterranean. The data is freely available for scientific purposes.

This methodology uses 4 channels of NOAA AVHRR and a physical relationship between surface temperature and NDVI. Though the known weaknesses of NOAA AVHRR the unmixing approach represents a technique potentially mitigating base data uncertainty by redistribution onto more channels and its relationships.

One of the added values of this technique is the outcome of endmember abundances, each of them utilizable as standalone products or in combination. In fact, the cold abundance was used to normalize GVF for 'undesired effects', mainly stemming from poor atmospheric conditions. In contrast to a simple NDVI, the positive effect of the cold abundance, improving the GVF, could be clearly shown. Moreover, the abundances represent subpixel information, exploiting further the limited NOAA AVHRR potentialities.

In this investigation, in comparison to a scaled NDVI, it could not be found a higher sensitivity of GVF for scarcely vegetated areas, as this was expected. However, the higher sensitivity is certainly given in comparison to a non-scaled NDVI, due to the extended range of GVF, exploiting the full margin within statistically derived limits.

It could be shown that the GVF is closer to the FAPAR data set than NDVI data. Considering the stability of FAPAR data for the investigated region and time period, GVF data, since it is less affected by extremes, can be considered as a more robust and hence a more reliable data set than NDVI. The applied unmixing technique can contribute to an improved data set, which is especially important for an accurate trend analysis.

As literature studies and our own analyses showed, GVF is still not a real fractional vegetation cover, as it contains also volumetric information about vegetation (similar to NDVI). An approximation of a real fractional vegetation fraction may be derived by squaring the GVF. Validation with independently derived data showed good agreement.

Acknowledgments

References

Adams, J. B. and Smith, M. O. Johnson P. E., 1986. Spectral mixture modelling: A new analysis of rock and soil types at the Viking Lander 1 Site. Journal of Geophysical Research, 91, B8, 8098-8112

Baret, F., Hagolle, O., Geiger, B., Bicheron, P., Miras, B., Huc, M., Berthelot, B., Nin?o, F., Weiss, M., Samain, O., Roujean, J. L., and Leroy, M., 2007. LAI, fAPAR and fCover CYCLOPES global products derived from VEGETATION. Part 1: Principles of the algorithm. Remote Sensing of Environment, 110, 3, 275-286

Billing, H., 2007. Land surface temperature corrected for orbital shift for evaluation test sites, Desurvey D1.5.1.14

Bolle, H.-J., Eckardt, M., Koslowsky, D., Maselli, F., Melia-Miralles, J., Menenti, M., Olesen, F.-S., Petkov, L., Rasool, L., and van de Griend, A., 2006. Mediterranean land-surface processes assessed from space, Springer, Berlin

Carlson, T. N. and Ripley, D. A., 1997. On the relation between NDVI, fractional vegetation cover, and leaf area index. Remote Sens.Env., 62, 241-252

Caselles, V. and Sobrino, J. A., 1989. Determination of frosts in orange groves from NOAA-9 AVHRR data. Remote Sens.Env., 29, 23-26

Chen, J., Jönsson, P., Tamura, M., Gu, Z., Matsushita, B., and Eklundh, L., 2004. A simple method for reconstructing a high-quality NDVI time-series data set based on the Savitzky-Golay filter. Remote Sens.Env., 91, 332-344

Choudhury, B. J., 1989. Estimating evaporation and carbon assimilation using infrared temperature data: vistas in modelling., 628-690, Asrar, G., Ed(s), Theory and Applications of Optical Remote Sensing, Wiley and sons, New York

Choudhury, B. J., Ahmed, N. U., Idso, S. B., Reginato, R. J., and Daughtry, C. S. T., 1994. Relations between evaporation coefficients and vegetation indices studied by model simulations. Remote Sens.Env., 50, 1-17

Coll, C. and Caselles, V., 1997. A split-window algorithm for land surface temperature from advanced very high resolution radiometer data: Validation and algorithm comparison. Journal of Geophysical Research, 102, D14, 16.697-16.713

Coll, C., Caselles, V., Sobrino, J. A., and Valor, E., 1994. On the atmospheric dependence of the split-window equation for land surface temperature. International Journal of Remote Sensing, 15, 105-122

Czajkowski, K. P., Goward, S. N., Mulhern, T., Goetz, S. J., Walz, A., Shirey, D., Stadler, S., Prince, S. D., and Dubayah, R. O., 2004. Estimating environmental variables using thermal remote sensing, 11-32, Quattrocchi, D. A. and Luvall, J. C., Ed(s), Thermal remote sensing in land surface processes, CRC Press

EEA, 11-12-2004. CORINE land cover changes 1990 - 2000 by country. http://dataservice.eea.europa.eu/atlas/viewdata/viewpub.asp?id=857. 7-9-2007

EEA, European Environment Agency, 3-2-2006. Corine land cover 2000 (CLC2000) 100 m - version 8/2005. http://dataservice.eea.europa.eu/dataservice/metadetails.asp?id=822. 1-2-2007

Eidenshink, J., 2008. A 19-year time series of 1-km AVHRR satellite data of the conterminous United States and Alaska. http://wwa.colorado.edu/current_projects/jeff_eidenshink2.pdf. 9-6-2008

European Commission, 1998. An integrated approach to assess and monitor desertification processes in the Mediterranean basin (DeMon-II). Final Report., Contract no.: 11589-95-12 A2 FP ISP B, Directorate General Joint Research Centre, Ispra

Gates, D. M., 1980. Biophysical Ecology, Springer Verlag, New York, Heidelberg, Berlin

Gillies, R. R. and Carlson, T. N., 1995. Thermal remote sensing of surface soil water content with partial vegetation cover for incorporation into climate models. Journal of Applied Meteorology, 34, 745-756

Gobron, N., Pinty, B., Verstraete, M. M., and Widlowsky, J.-L., 2000. Advanced Vegetation Indices Optimized for Up-Coming Sensors: Design, Performance and Applications. IEEE Transactions on Geoscience and Remote Sensing, 38, 2489-2505

Goward, S. N. and Hope, A. S., 1989. Evapotranspiration from combined reflected solar and emitted terrestrial radiation: Preliminary FIFE results from AVHRR data. Advances in Space Research, 9, 239-249

Gutman, G. and Ignatov, A., 1998. The derivation of the green vegetation fraction from NOAA/AVHRR data for use in numerical weather prediction models. International Journal of Remote Sensing, 19, 8, 1533-1543

Hill, J., Mégier, J., and Mehl, W., 1995. Land degradation, soil erosion and desertification monitoring in mediterranean ecosystems. Remote Sensing Rev., 12, 107-130

Holben, B. N., 1986. Characterization of maximum value composites from temporal AVHRR data. International Journal of Remote Sensing, 7, 1417-1434

Huete, A. R., 1988. A soil-adjusted vegetation index (SAVI). Remote Sensing Environment, 25, 295-309

Huete, A. R., Jackson, R. D., and Post, D. F., 1987. Spectral response of a plant canopy with different soil backgrounds. Remote Sens.Env., 17, 37-53

Koslowsky, D., 1998. Daily extended 1-km AVHRR data sets of the Mediterranean, Proceedings 9th Conf.Sat.Meteror.and Oceanogr., 25-29 May

Koslowsky, D., 2003. 12 years mediterranean satellite data set and analysis, 165-177, Bolle, H.-J., Ed(s), Mediterranean Climate, Springer Verlag, Berlin, Heidelberg, New York

Koslowsky, D., Billing, H., and Eckardt, M., 2001. Sensor degradation and inter-calibration of the shortwave channels of the AVHRR - NOAA 11/14/16 satellites, Proceedings of the 2001 EUMETSAT Meteorological satellite data user's conference, 107-113

Koslowsky, D., Billing, H., and Friedrich, K., 2005. MEDOKADS: A long-term data set for detection and monitoring of desertification risks in the Mediterranean. Remote Sensing and Geoinformation in the assessment and monitoring of land degradation and desertification, Roeder, A. and Hill, J., RGLDD, Trier, Germany, 191-198

Lambin, E. F. and Ehrlich, D., 1995. Combining vegetation indices and surface temperature for land-cover mapping at broad spatial scales. International Journal of Remote Sensing, 16, 3, 573-579

Lambin, E. F. and Ehrlich, D., 1996. The surface temperature-vegetation index space for land cover and land-cover change analysis. International Journal of Remote Sensing, 17, 3, 463-487

Lohninger, H., 1999. Teach/Me Data Analysis, Springer Verlag, Berlin

Medias France, 12-15-2006. CYCLOPES (Carbon cYcle and Change in Land Obeservational Products from an Ensemble of Satellites) EGV2-2001-00035 (FP5)- Products read me

Myneni, R. B., Asrar, G., Tanre, D., and Choudhury, B. J., 1992. Remote sensing of solar radiation absorbed and reflected by vegetation land surfaces. IEEE Transactions on Geoscience and Remote Sensing, 30, 302-314

Nemani, P., Pierce, L., Running, S. W., and Goward, S., 1993. Developing satellite derived estimates of surface moisture status. Journal of Applied Meteorology, 32, 548-557

Pinty, B. and Verstraete, M. M., 7-1-1992. GEMI: a non-linear index to monitor global vegetation from satellites. Plant Ecology, 101, 1, 15-20

Price, J. C., 1993. Estimating leaf area index from satellite data. IEEE Transactions on Geoscience and Remote Sensing, 31, 3, 727-734

Sandholt, I., Rasmussen, K., and Andersen, J., 2002. A simple interpretation of the surface temperature/vegetation index space for assessment of surface moisture status. Remote Sensing of Environment, 79, 2-3, 213-224

Singh, S. M., 1988. Simulation of solar zenith angle effect on global vegetation index (GVI) data. International Journal of Remote Sensing, 9, 2, 237-248

Smith, Milton O., Ustin, Susan L., Adams, John B., and Gillespie, Alan R., 1990. Vegetation in deserts: I. A regional measure of abundance from multispectral images. Remote Sensing of Environment, 31, 1, 1-26

Sommer, S., 1999. Regional desertification indicators. Final report MEDALUS III, ENV4-CT95-0121

Stellmes, M., Sommer, S., and Hill, J., 2005. Use of the NOAA AVHRR NDVI-Ts feature space to derive vegetation cover estimates from long term time series for determining regional vegetation trends in the Mediterranean. Remote Sensing and Geoinformation Processing in the Assessment and Monitoring of Land Degradation and Desertification, Trier, Germany, 231-238

Trishchenko, A. P., Cihlar, J., and Zhanqing, L., 2002. Effects of spectral response function on surface reflectance and NDVI measured with moderate resolution satellite sensors. Remote Sens.Env., 81, 1-18

Udelhoven, T., 2006. TimeStats: a software tool for analyzing spatial-temporal raster data archives, 1st Conference on Remote Sensing and Geoinformation Processing in the Assessment and Monitoring of Land Degradation and Desertification, Trier, Germany

Abstract

NOAA AVHRR data stemming from the MEDOKADS archive and ranging from 1989 to 2005 was processed and decomposed into their fractions of the vegetated, non-vegetated and the so called 'cold' endmember. Decomposition occurred via Linear Unmixing within a triangle spanned up by NDVI (y-axis) and surface temperature (x-axis), separately for each of the 612 10-day composites. Endmembers were derived statistically using percentiles and the inverse relationship between NDVI and Ts. The cold endmember was fixed at -20 degrees Celsius, the vegetated endmember at NDVI = 0.7, the latter was then empirically corrected for illumination effects. Linear Unmixing occurred for the whole Mediterranean area, separately for a western and eastern window. Outcomes are the vegetation abundance, soil abundance and 'cold' abundance, indicating the individual coverage of a pixel by each of these. The vegetation abundance was re-scaled to the so-called Grenn Vegetation Fraction (GVF), re-distributing the "cold" abundance on vegetation and soil abundance proportionally. Unmixing led to a higher stability of GVF data in comparison to NDVI data with regard to atmospheric effects. The data was post-processed for missing values and outliers and it was filtered. The GVF shows close parallelism on several test sites in comparison to a re-scaled NDVI within the endmember limits. The positive effect of the cold abundance, which is amongst other accounting for negative effects from poor atmospheric conditions and which was used to improve the GVF, could be clearly shown. Comparison with high and low resolution SPOT data shows a linear relationship and higher values for GVF. Squared GVF values were found to be closely correlated with independently derived high and low resolution vegetation cover (fCover), confirming this relationship known from literature. Coefficients of determination (R^2), slope and offset of linear relations between squared GVF on one side and the two validation data sets on the other side were 0.69, 0.91, 0.07 and 0.58, 1.27, 0.06, respectively. In addition to the 'per se' value of the derived abundances, validation results indicate that squared GVF may be used as approximation for vegetation cover.

How to obtain EU publications

Our priced publications are available from EU Bookshop (http://bookshop.europa.eu), where you can place an order with the sales agent of your choice.

The Publications Office has a worldwide network of sales agents. You can obtain their contact details by sending a fax to (352) 29 29-42758.

The mission of the JRC is to provide customer-driven scientific and technical support for the conception, development, implementation and monitoring of EU policies. As a service of the European Commission, the JRC functions as a reference centre of science and technology for the Union. Close to the policy-making process, it serves the common interest of the Member States, while being independent of special interests, whether private or national.

JRC
EUROPEAN COMMISSION

Publications Office
Publications.eu.int